PFC/JA-81-18

Nonlinear Coupling to Lower Hybrid Waves in a Tokamak Plasma

Kim Theilhaber

Plasma Fusion Center
Massachusetts Institute of Technology
Cambridge, MA 02139

September 1981

NONLINEAR COUPLING TO LOWER HYBRID WAVES IN A TOKAMAK PLASMA

Kim Theilhaber

Plasma Fusion Center
Massachusetts Institute of Technology
United States of America

Abstract

The nonlinear coupling of lower hybrid waves excited by a waveguide array is examined numerically and analytically in a model of a Tokamak plasma. The nonlinearity considered is the ponderomotive force and the fields are evolved self-consistently in time to the steady-state. Simplified coupling models are derived for the loading of large and small arrays and for different phasings of the waveguides. It is found that the reflection coefficient can be modified considerably by the nonlinear effects. It is also found that the nonlinear modification of the power spectrum is especially large when the array excites two resonance cones. The fields filament and the spectrum is broadened and upshifted. The travelling-wave excitation, which excites a single resonance cone and is considered for current drive, is less affected nonlinearly; the fields do not filament and the spectrum remains narrow.

1. Introduction

In this paper we study how nonlinear effects modify the coupling of a waveguide array which excites lower hybrid waves in a Tokamak plasma. The nonlinearity considered is that of the "ponderomotive force" exerted by the RF fields. This force creates density depressions in the plasma, and results in a nonlinear modification of the loading of the waveguides. It also modifies the power spectrum of waves excited inside the plasma, that is their distribution in the parallel wave index $n_z = \frac{ck_z}{\omega}$. The ponderomotive force becomes important when the oscillation energy of the particles in the electric field becomes comparable to their thermal energy. Because of the low edge temperatures in the plasma (a few electron volts) the ponderomotive force is sizeable even for moderate power densities, say 1 kW/cm^2.

The aim of this paper is to examine a number of representative excitations, and to gauge numerically and analytically the importance of nonlinear effects in each case. Of prime interest is the effect of the finite parallel extent of the excitation, an effect not included in previous treatments of the problem. The importance of the parallel modulation has been pointed out by Bers[1].

To summarize results, it is found that the plasma admittance presented to the waveguides can be substantially modified at large powers. The effects are more pronounced if the density gradient is weak or if the excitation spectrum is wide in k_z space. We also found that the power spectrum can be changed appreciably because the fields self-focuse and filament in real space, and this results in a broadening of the spectrum. These nonlinear effects are more pronounced for the standing-wave excitation. For the travelling wave, the power spectrum remains unidirectional and narrow.

Though the basic work is numerical, we derive simplified analytic models to compute the nonlinear loading of the waveguides. We consider three types of excitation: (I) a large travelling-wave array, (II) a large standing-wave array, and (III) a two-waveguide array. In each case we find a relatively simple "coupling equation", and compared its predictions with the full numerical solution of the nonlinear lower hybrid equation.

The numerical approach is to evolve in time the propagation equations of the lower hybrid waves so as to achieve a steady-state. With such an approach causality in the solutions is automatically satisfied. A similar method has been used in the solution of the Complex Modified Korteweg deVries equation[2], though in that case a steady state was not necessarily obtained.

Previous work on nonlinear effects in propagation is of limited applicability, because the edge region in front of the waveguides is either excluded from the analysis or because only a simplified excitation is considered. For instance, a nonlinear Schroedinger equation or a "Complex Modified Korteweg deVries" equation can be derived to describe the modification of a single lower hybrid resonance cone[3,4,5]. However this formulation does not predict the waveguide loading, which depends to a large extent on the edge region where both resonance cones interact, and it also assumes weak nonlinearity, an assumption which is not valid near the edge at large power densities. In treating the edge region, only travelling-wave excitations have been considered [6,7,8], and this requires a narrow and unidirectional parallel wave spectrum. Such a spectrum would be produced by a large array with $\frac{\pi}{2}$ progressive phasing. Other phasings are excluded from the analysis.

The importance of assuming a travelling wave excitation is that it eliminates the parallel z coordinate from the propagation equations. The problem becomes one-dimensional in space, and this is a great simplification. Morales[6] has looked at the time-dependent problem for the coupling of an infinite travelling-wave excitation. The results of his numerical calculation show that a steady-state is not achieved, but rather that energy is coupled into the plasma through a quasi-periodic

series of bursts of wave packets. It should be noted however that the exponent used by Morales for the nonlinear density is not correct, as it incorporates the equilibrium density in a denominator. This overestimates the amplitude of the nonlinearity at the low densities, where the denominator goes to zero. Furthermore, the work of Chan and Chiu[7], and of Fukuyama et al.[8], shows that steady states to the travelling-wave excitation do exist and can be evaluated numerically.

In this paper, we go beyond the travelling wave theory of refs.[7,8] and emphasize the two-dimensional nature of the edge problem by studying excitations of finite extent in z. To do this, we must solve the "Nonlinear Klein Gordon Equation", derived by Krapchev and Bers[9]. An analytic treatment of this equation has been given by Krapchev et al.[10], but under the assumption that the perpendicular dependence of the density modulation can be neglected. The numerical results of the present paper indicate that this assumption may not be valid. In Section 7 we present a simplified coupling equation which accounts for the perpendicular dependence of the density modulation, and which produces results in agreement with the numerical solution of the Nonlinear Klein Gordon Equation.

Several investigators are at present engaged in the numerical solution of the coupling problem [11,12,13]. Their work both parallels and complements the approach of the present paper[14].

2. Basic Equations

The geometry for the coupling is shown in fig.(1). A slab geometry is used, with z in the direction of the toroidal magnetic field and x in the direction of the density gradient. The system is assumed uniform in y, and the waveguides are modeled by parallel plates infinite in the y direction. The TM mode is excited so that at the waveguide apertures the electric field E is in the xz plane.

In fig.(1) we indicate the boundaries of the "coupling region", the region which determines the loading of the waveguides and in which the ponderomotive nonlinearity is large. This region extends from the waveguide mouths to just beyond the limiter shadow. We model the edge conditions[15] by taking the density profile as linear and by assuming the temperature is constant ($T_{e,i} = 1 - 5$ eV) up to the limiter shadow, beyond which it rises rapidly. Roughly, we concentrate on a region which extends a few free-space wavelengths in z (say 20-30 cm) and of extent 1-3 cm in x.

To derive an evolution equation for the electric field we decompose $\mathrm{E}(\mathrm{r}, t)$ into fast and slow components[6]:

$$\mathrm{E}(\mathrm{r}, t) = \hat{\mathrm{E}}(\mathrm{r}, t)e^{-i\omega_0 t} + c.c. \tag{1}$$

where $\hat{\mathrm{E}}$ is slowly-varying in time and ω_0 is the source frequency. Expanding Maxwell's equations yields:

$$\nabla \times \nabla \times \hat{\mathrm{E}} = \frac{1}{c^2}\left(\omega^2 \mathrm{K}(\omega) \cdot \hat{\mathrm{E}} + i\frac{\partial}{\partial\omega}(\omega^2 \mathrm{K}) \cdot \frac{\partial \hat{\mathrm{E}}}{\partial t} + \ldots\right)_{\omega=\omega_0} \tag{2}$$

where $\mathrm{K}(\omega)$ is the cold-plasma dielectric tensor[16]. We neglect thermal dispersion in this high frequency equation. For lower hybrid waves, we have $\Omega_i \ll \omega_0 \ll \Omega_e$, where $\Omega_{e,i}$ are the cyclotron frequencies, and in the low-density coupling region $\omega_{pe}(x) \ll \Omega_e$, $\omega_{pi}(x) \ll \omega_0$, where $\omega_{pe,pi}$ are the plasma frequencies. With the approximations allowed by these conditions, and assuming that $E_y = 0$ and $\partial/\partial y = 0$, we find to first order in $\partial/\partial t$:

$$i\frac{\partial \hat{E}_x}{\partial \tau} + \left(\frac{\partial^2}{\partial z^2} + 1\right)\hat{E}_x - \frac{\partial^2 \hat{E}_z}{\partial x \partial z} = 0 \tag{3}$$

$$i\frac{\partial \hat{E}_z}{\partial \tau} + \left(\frac{\partial^2}{\partial x^2} + K_{\|}\right)\hat{E}_z - \frac{\partial^2 \hat{E}_x}{\partial x \partial z} = 0 \tag{4}$$

where space and time have been normalized, $\mathrm{r} \rightarrow \frac{\omega_0}{c}\mathrm{r}$ and $\tau = \frac{\omega_0}{2}t$. In eqs.(3,4) the nonlinear term is the parallel element of the dielectric tensor, $K_{\|} = 1 - \frac{\omega_{pe}^2(n_e)}{\omega_0^2}$, where n_e is the local electron density which is modulated by the ponderomotive force.

As noted in the introduction, we construct evolution equations chiefly to obtain a steady-state. In so doing, we neglect the details of the low-frequency dynamics and assume the ponderomotive density modulation is produced instantaneously.

A general expression for the ponderomotive potential is given in [17]. In the coupling region we have $E_y = 0$, $E_x \simeq E_z$. With these magnitudes the electrons are assumed infinitely magnetized, with ponderomotive potential:

$$\phi_{pe} = \frac{e^2}{4m_e\omega^2}|\hat{E}_z|^2 \tag{5}$$

and the ponderomotive force on the ions is negligible, $\phi_{pi} \simeq \frac{m_e}{m_i}\phi_{pe}$. We assume quasineutrality and an electrostatic potential and balance low-frequency electric and ponderomotive forces with the thermal pressure for both the electrons and the ions. After some elimination this yields the steady-state density modification:

$$n_e = n_i = n_0(x)\exp\left(-\frac{e^2|\hat{E}_z|^2}{4m_e\omega^2(T_e+T_i)}\right) \tag{6}$$

We define:

$$\mathrm{E} = \left(\frac{e^2}{4m_e(T_{e0}+T_{i0})}\right)^{1/2}\hat{\mathrm{E}} \tag{7}$$

$$\beta(x) = \frac{T_{e0}+T_{i0}}{T_e(x)+T_i(x)} \tag{8}$$

$$A_0(x) = \frac{\omega_{pe0}^2(x)}{\omega^2} \tag{9}$$

where E now denotes a normalized electric field. The factor $\beta(x)$ allows for a nonuniform temperature, and we define $T_{e,i0} \equiv T_{e,i}(0)$. The density term is $A_0(x) = \frac{\omega_{pe0}^2(x)}{\omega^2}$, which is proportional to the equilibrium density. Eqs.(3,4) become:

$$i\frac{\partial E_x}{\partial\tau} + \left(\frac{\partial^2}{\partial z^2}+1\right)E_x - \frac{\partial^2 E_z}{\partial x\partial z} = 0 \tag{10}$$

$$i\frac{\partial E_z}{\partial\tau} + \left(\frac{\partial^2}{\partial x^2}+1-A_0(x)e^{-\beta(x)|E_z|^2}\right)E_z - \frac{\partial^2 E_x}{\partial x\partial z} = 0 \tag{11}$$

Where E is the normalized electric field. Finally, we simplify eqs.(10,11) by eliminating E_x. This can be done by noting from eq.(10) that $(i\partial_\tau + \partial_x^2 + 1)E_x = \partial_{xz}^2 E_z$. Multiplying eq.(11) by the operator $(i\partial_\tau + \partial_x^2 + 1)$ and interchanging this operator with ∂_{xz}^2 yields the term $\partial_x^2\partial_z^2 E_z$. Expanding the other terms yields:

$$\begin{aligned} -\frac{\partial^2 E_z}{\partial\tau^2} + i\frac{\partial}{\partial\tau}\left(\left(\frac{\partial^2}{\partial z^2}+1+\frac{\partial^2}{\partial x^2}+K_{\|}\right)E_z\right) \\ + \frac{\partial^2 E_z}{\partial x^2} + \left(\frac{\partial^2}{\partial z^2}+1\right)(K_{\|}E_z) = 0 \end{aligned} \tag{12}$$

We neglect ∂_τ^2, and also, to lowest order, we note that $\partial_x^2 E_z \simeq -(\partial_z^2 + 1)(K_{||} E_z)$. This results in the final equation:

$$i\frac{\partial}{\partial\tau}\left(E_z + \frac{\partial^2}{\partial z^2}\left(A_0(x)e^{-\beta(x)|E_z|^2}E_z\right)\right) + \frac{\partial^2 E_z}{\partial x^2} - \left(\frac{\partial^2}{\partial z^2}+1\right)\left(\left(A_0(x)e^{-\beta(x)|E_z|^2}-1\right)E_z\right) = 0 \tag{13}$$

In the steady-state, the time-derivative term disappears:

$$\frac{\partial^2 E_z}{\partial x^2} - \left(\frac{\partial^2}{\partial z^2}+1\right)\left(\left(A_0(x)e^{-\beta(x)|E_z|^2}-1\right)E_z\right) = 0 \tag{14}$$

and it is the solution of this "Nonlinear Klein-Gordon Equation"[9], that we shall be seeking by evolving eq.(13) numerically to the steady-state. We shall refer to eq.(14) as the "2D" equation as it incorporates both z and x modulation of the fields. In Appendix A, we show the connection of eq.(14) with the equations derived for weak nonlinearity and a single resonance cone[3,5], in other words for beyond the coupling region.

3. Complex Poynting Flux and Power Conservation

Eq.(14) has a simple conservation law. Writing the y component of Faraday's Law and using eq.(10) with $\partial/\partial\tau = 0$ to eliminate E_x, we find the steady-state magnetic field:

$$\left(\frac{\partial^2}{\partial z^2}+1\right)H_y = i\sqrt{\frac{\epsilon_0}{\mu_0}}\frac{\partial E_z}{\partial x} \tag{15}$$

We define a complex Poynting Flux:

$$P(x) = \int_{-\infty}^{\infty}\frac{1}{2}(-E_z H_y^*)\,dz = P_R(x) + iP_I(x) \tag{16}$$

From eq.(14) and (15) it can be shown that in the steady-state $\frac{d}{dx}P_R(x) = 0$. This is simply the conservation of time-averaged power flux. The quantity $P_I(x)$ is not conserved, but its value at the source, $P_I(0)$, is a measure of the reactive loading of the exciting structure.

4. Normalized Equation

We assume a linear density profile in the coupling region, so that in eq.(13) we have $A_0(x) = \frac{\omega_{pe0}^2(x)}{\omega^2} = \alpha x$, where $\alpha = \frac{d}{dx}\frac{\omega_{pe0}^2(x)}{\omega^2}\Big|_{x=0}$. The gradient parameter α is in general quite large. For example consider the ALCATOR-A experiment, with frequency $f = 2.45\,\mathrm{GHz}$. For this frequency, the cutoff density, determined by $\omega_{pe0} = \omega$, is $n_{0c} = 7.5 \times 10^{10}\mathrm{cm}^{-3}$. Let us assume an edge plasma where the density rises from being underdense, $n_{01} < n_{0c}$ to about 10% of the central density, say to $n_{02} = 10^{13}\mathrm{cm}^{-3}$. We assume this rise occurs in $\delta x_{real} = 0.5\,\mathrm{cm}$, which is consistent with probe measurements of the ALCATOR-A discharge[15]. With x normalized by k_0, we find $\delta x = k_0 \delta x_{real} = 0.256$, and $\alpha \simeq (n_{02}/n_{0c})/\delta x = 520$.

We also specify a temperature profile in the definition of the term $\beta(x)$ of eq.(13). We model the physical conditions by assuming that the temperature is constant in $0 < x < x_1$ and then that it rises to infinity in some range $x_1 < x < x_2$. Thus $\beta(x) = 1$ in $0 < x < x_1$, $\beta(x) = 0$ for $x > x_2$ and we define $\beta(x) \equiv (1 - (x - x_1)^2/(x_2 - x_1)^2)^2$ in $x_1 < x < x_2$.

It is convenient to normalize the density term. We write:

$$\xi = \alpha^{1/3} x \qquad\qquad a_0 = \frac{1}{\alpha^{2/3}} \tag{17}$$

and eq.(13) becomes:

$$i\frac{\partial}{\partial \tau}\left(\frac{\partial^2}{\partial z^2}(\xi e^{-\tilde{\beta}(\xi)|E_z|^2}E_z) + a_0 E_z\right) + \frac{\partial^2}{\partial \xi^2}E_z - \left(\frac{\partial^2}{\partial z^2} + 1\right)\left((\xi e^{-\tilde{\beta}(\xi)|E_z|^2} - a_0)E_z\right) = 0 \tag{18}$$

where $\tilde{\beta}(\xi) = \beta(x)$.

The term a_0 accounts for the presence of the cutoff layer. Since in general $\alpha \gg 1$, a_0 is negligible. This has the advantage of removing the explicit dependence of eq.(18) on the gradient parameter α, in the range $0 < \xi < \xi_1$. What remains is an implicit dependence on the extent of the nonlinear region in normalized space, the transition to the linear region occurring over $\xi_{1,2} = \alpha^{1/3} x_{1,2}$. It is found empirically that the waveguide loading is not very sensitive to the depth of the nonlinear region. Provided $\xi_{1,2} > 2$, the nonlinear plasma admittance is independent of the exact values of $\xi_{1,2}$. This is because at all but very large field amplitudes the plasma admittance is determined by a region close to the source. Of course, the spectrum of the waves exiting at the far end of the coupling region is very sensitive to the depth of the nonlinear region.

The numerical method of solution for eq.(18) is outlined in Appendix B. We evolve eq.(18) in time to the steady state, a procedure which usually takes about 150 time steps. All the numerical results which follow refer to this steady-state. As explained in Appendix B, a limitation of the numerical scheme is the lack of a physical mechanism to balance the effects of filamentation. We use a digital filter to limit peaking of the fields, and this entails a penalty in the form of artificial dissipation. We denote the fractional power loss due to this dissipation by ϵ_P.

5. Long Travelling Wave Array

A. Field Structure

To model a large array with progressive phasing $\frac{\pi}{2}$ we consider the excitation:

$$E(\xi=0,z)=\begin{cases} E_0\left(1-\left(\frac{z}{z_0}\right)^2\right)^2 e^{in_{z0}z}, & |z|<z_0 \\ 0, & |z|>z_0 \end{cases} \tag{19}$$

The spectrum of this excitation is centered about $n_z = n_{z0}$ and has small sidelobes. If b is the individual waveguide width, then we have $n_{z0} = \frac{\pi}{2b}$.

In fig.(2a) we show the linear field structure ($|E(\xi,z)|$ plotted for $E_0 \ll 1$) for $n_{z0} = 2.0$ and $z_0 = 4.0$. For $n_{z0} = 2.0$ the waveguide width is $b \simeq 0.8$ and there are roughly $\frac{2z_0}{b} \simeq 10$ waveguides in the array.

The linear fields follow a resonance cone roughly symmetric about its axis. Asymmetry comes from electromagnetic dispersion which spreads waves with $n_z \simeq 1$ to larger z. The center of the resonance cone follows closely the ray trajectory:

$$z_{\text{ray}} = \int_0^{\xi}\left(-\frac{\partial n_x}{\partial n_z}\right)d\xi' = \frac{2}{3}\frac{n_{z0}}{(n_{z0}^2-1)^{1/2}}\xi^{3/2} \tag{20}$$

As we turn up the field amplitude at the edge, there are noticeable effects on the propagation in real space (fig.(2b)). The peak of the resonance cone penetrates into the plasma at a steeper angle to the magnetic field (it travels less in z to reach a given ξ). The shape of the resonance cone is distorted, displaying a "shock front" in the cross-section of the envelope. That this should happen is not surprising. In regions where the density is depressed, because of the high fields, the ray trajectories are steeper, and they intersect with rays issued from regions of more moderate fields. The convergence of the different rays leads to the formation of the shock.

The power spectrum is defined by:

$$P(\xi, n_z) = \frac{1}{2}\mathrm{Re}(-\tilde{E}(\xi, n_z)\tilde{H}^*(\xi, n_z)) \tag{21}$$

In linear propagation, power in each n_z is conserved, and we have $P(\xi, n_z) =$ constant. This is not the case in nonlinear propagation. In Fourier space we see the spectrum broaden with a power transfer to both higher and lower n_z. However, the spectrum remains unidirectional, that is a negligible amount of negative n_z's are generated and the transfer to lower n_z is essentially limited to values above 1. The spectrum also exhibits a "tail" to larger n_z, but this tail does not carry very much power. This can be seen in fig.(3), where we graph together the linear and nonlinear power spectrum for $\xi = 3.5$.

We define $< n_z >$ as the center of gravity of the power spectrum in positive n_z:

$$< n_z > \equiv \frac{\int_0^\infty n_z P(n_z)\, dn_z}{\int_0^\infty P(n_z)\, dn_z} \tag{22}$$

Using $< n_z >$ as a measure, we find that the overall shift is downward, $\delta < n_z > \simeq -0.1$. Varying z_0 and n_{z0} in the ranges $1.0 < n_{z0} < 3.0$ and $2.0 < z_0 < 8.0$, we find that in all cases the downshift is modest, with $-0.5 < \delta < n_z >< -0.1$. The fractional power loss to the numerical filter remained small, with $\epsilon_P < 0.05$.

The discussion above applies to a narrow spectrum centered about some $n_{z0} > 1$. Reducing n_{z0} or broadening the spectrum by decreasing z_0 results in increased electromagnetic dispersion, with a tail forming on the resonance cone which spreads the fields to larger z. However the nonlinear field structure remains qualitatively the same, provided the spectrum in $n_z < -1$ is small. When the excitation in $n_z < -1$ is not initially small, there is strong coupling between $n_z > 1$ and $n_z < -1$ components, and the spectrum is more strongly modified. We examine this situation in Section 6.

B. Coupling Equation

From eq.(18) we calculated numerically the complex Poynting flux $P(0)$ coupled at the source and compared results of our computation with those of the simpler model of refs.[7,8]. As a refinement to this model, we allowed for the finite width of the envelope by writing:

$$P(0) = \frac{1}{2}\int_{-\infty}^{\infty} Y_f^*(z)\hat{E}_0^2(z)\, dz \tag{23}$$

where $\hat{E}_0(z) = |E(0,z)|$ is the envelope function. For simplicity, we omit a factor of $\sqrt{\frac{\epsilon_0}{\mu_0}}$. All admittances are normalized to the free-space value, $Y_0 = \sqrt{\frac{\epsilon_0}{\mu_0}} = \frac{1}{377}\Omega^{-1}$. In particular, the admittance of the fundamental parallel plate waveguide mode is 1. The admittance $Y_P(z)$ is found for a given $z = z_1$ by considering the excitation at that point to be an infinite travelling wave with constant amplitude $\hat{E}_0(z_1)$. The admittance is then found from $Y_P = \alpha^{1/3}\frac{i}{n_{z0}^2-1}\frac{1}{E_1}\frac{dE_1}{d\xi}$, where E_1 is the solution of the infinite travelling-wave equation:

$$\frac{d^2E_1}{d\xi^2} + (n_{z0}^2 - 1)\xi e^{-|E_1|^2}E_1 = 0, \qquad E_1(\xi = 0) = \hat{E}_0(z) \tag{24}$$

This ordinary differential equation is solved numerically by assuming radiation conditions at $\xi \to \infty$. We refer to eq.(24) as the "1D" equation.

Results of the 2D and 1D calculations are compared in fig.(4) for the case $n_{z0} = 2.0$ and $z_0 = 4.0$, which represents a ten-waveguide array. The discrete points result from the 2D calculation, the curves are obtained from eq.(24). There is good agreement up to quite large edge amplitudes, and this confirms the validity of one dimensional model for the coupling of this array.

The 1D model is valid provided the array is "large", and in practice we find this means it must contain at least six elements. The coupling of a smaller four-waveguide array with $\frac{\pi}{2}$ phasing is still qualitatively described by eq.(24) provided $n_{z0} = \frac{\pi}{2b}$ is not too close to 1; roughly, we require that $n_{z0} > 3$. For $n_{z0} < 3$, we have had success with the coupling model described in Section 7.

Having gained confidence that eq.(24) is valid, we can match waveguides to plasma and obtain the reflection coefficient $|R|^2$ as a function of incident power. This has been done in ref.[8]. It is found that for most density gradients $|R|^2$ increases with incident power.

6. Long Standing Wave Array

A. Coupling Equation

When the large array is phased by π, the excitation spectrum has two narrow peaks centered about $n_z = \pm n_{z0}$ where now $n_{z0} \simeq \frac{\pi}{b}$. We model the excitation by:

$$E(\xi = 0, z) = \hat{E}_0(z)\cos(n_{z0}z) \tag{25}$$

where $\hat{E}_0(z)$ is some envelope function. For numerical experimentation it may be chosen smooth as in eq.(19). More realistically, $\hat{E}_0(z) = E_0 =$ constant in front of the waveguide mouths (assuming the same amplitudes in all the waveguides) and $\hat{E}_0(z) = 0$ everywhere else.

We derive below a simplified one-dimensional coupling equation for the standing wave excitation. The first simplification is to assume that the envelope is of infinite extent. We then consider a periodic excitation at $\xi = 0$ and assume Fourier series for the fields and the nonlinear term:

$$E(\xi, z) = \sum_{n=-\infty}^{\infty} \mathcal{E}_n(\xi) e^{inn_{z0}z}, \qquad e^{-|E(\xi,z)|^2} = \sum_{n=-\infty}^{\infty} F_n(\xi) e^{inn_{z0}z} \tag{26}$$

With the boundary condition $\mathcal{E}_n(0) \equiv \mathcal{E}_{n0}$. The coefficients F_n have a complicated functional dependence on $|E(\xi, z)|^2$. The Fourier components of eq.(18) are:

$$\frac{d^2\mathcal{E}_n}{d\xi^2} + k_n^2 \xi F_0 \mathcal{E}_n + k_n^2 \xi \sum_{m \neq 0} F_m \mathcal{E}_{n-m} = 0 \tag{27}$$

where $k_n = (n^2 n_{z0}^2 - 1)^{1/2}$.

The system of equations (27) is hard to solve, even numerically and in a truncated form. In what follows, we simplify them drastically and obtain results for the complex power coupled, if not for the fields deep inside the plasma. We consider the excitation corresponding to eq.(25), $E(0, z) = 2\mathcal{E}_{10} \cos(n_{z0}z)$. If we assume this field pattern remains dominant inside the plasma, the density modulation is given by[10]:

$$e^{-|E(\xi,z)|^2} \simeq e^{-4|\mathcal{E}_1(\xi)|^2 \cos^2(n_{z0}z)} = \sum_{m=-\infty}^{\infty} F_{2m} e^{i2mn_{z0}z} \tag{28}$$

$$F_{2m} = \exp(-2|\mathcal{E}_1|^2) \mathrm{I}_m(2|\mathcal{E}_1|^2)$$

where I_m is the m-th modified Bessel function. Note that only even harmonics of $\exp(in_{z0}z)$ are present, and that these terms couple only odd harmonics of $\mathcal{E}_n$. This occurs even when the approximation of eq.(28) is not made, provided that in eq.(26) $\mathcal{E}_{-n} = \mathcal{E}_n$.

The expansion of eq.(28) is used by Krapchev et al.[10] in their treatment of waveguide coupling, but it is assumed in their derivation that $\mathcal{E}_1(\xi) =$ constant. We retain here the ξ dependence of $\mathcal{E}_1$, while ignoring the effect of harmonic generation on the waveguide loading. We do this by

neglecting in eq.(27) all but the $m = \pm 1$ harmonics. Such an assumption is consistent with the approximation of the nonlinear term in eq.(28). This yields the coupling equation:

$$\frac{d^2\mathcal{E}_1}{d\xi^2} + (n_{z0}^2 - 1)\xi e^{-2|\mathcal{E}_1|^2}\Big(\mathrm{I}_0(2|\mathcal{E}_1|^2) - \mathrm{I}_1(2|\mathcal{E}_1|^2)\Big)\mathcal{E}_1 = 0, \quad \mathcal{E}_1(\xi = 0) = \mathcal{E}_{10} = \frac{1}{2}E_0 \quad (29)$$

where we assume an infinite nonlinear region. This equation is very similar to the one-dimensional equation derived for the travelling-wave excitation, eq.(24). It merely has a more complicated "effective" density modification. We expect it to be valid only close to the source, where there has not been much cascading into the higher harmonics. Thus eq.(29) is primarily an equation to predict coupling, and does not show what happens to the spectrum inside the plasma.

Eq.(29) gives us the "local" plasma admittance, $Y_P(z) = \alpha^{1/3}\frac{i}{n_{z0}^2-1}\frac{1}{\mathcal{E}_1}\frac{d\mathcal{E}_1}{d\xi}$, where $\mathcal{E}_1$ is obtained from eq.(29) with the boundary condition $\mathcal{E}_1(\xi = 0) = \frac{1}{2}\hat{E}_0(z)$. We allow for a finite envelope by weighing as before:

$$P(0) = \frac{1}{4}\int_{-\infty}^{\infty} Y_P(z)\hat{E}_0^2(z)\,dz \quad (30)$$

where a factor of $\frac{1}{2}$ comes from averaging over the $\cos^2(n_{z0}z)$ term.

Results for power coupled are compared in fig.(5) for a four-waveguide array, with $b = 1.5$. The discrete data points are the results of the 2D integration, the continuous curves were obtained from the 1D model, eq.(29). There is fair agreement up to $E_0 = 3.0$, beyond which the reactance from the 2D model increases more rapidly than predicted by the 1D model. This is probably because the 1D model does not account for the finite extent of the nonlinear region, and the transition to the linear region leads to increased reflection at large amplitudes.

We can apply eq.(29) to waveguide coupling. The reflection coefficient is given by $|R|^2 = \left|\frac{1-Y_P}{1+Y_P}\right|^2$ where Y_P is obtained from eq.(29) with $n_{z0} = \frac{\pi}{b}$. Because of the scaling of eq.(29), Y_P can be written $Y_P = Q\hat{Y}_P$ where $Q = \alpha^{1/3}/(n_{z0}^2 - 1)^{2/3}$ and where $\hat{Y}_P$ is independent of α and n_{z0}. The results are shown in fig.(6), where $|R|^2$ is plotted as a function of the incident field amplitude. The behavior of $|R|^2$ for the standing wave excitation is very similar to that of the travelling wave. In most cases the reflectivity increases considerably with increasing incident power.

B. Field Structure

Linear and nonlinear field structures are shown in figs.(7). The excitation is eq.(25), with $\hat{E}_0(z) = \left(1 - (z/z_0)^2\right)^2$, and $n_{z0} = 1.7$, $z_0 = 6.0$. This corresponds to a four-waveguide array.

The strong filamentation seen in fig.(7b) corresponds to generation of odd harmonics in Fourier space. This can be seen in fig.(8). The peaks of the linear spectrum occur roughly at $n_z = \pm 1.7$, and in the nonlinear regime we see growth of the Fourier components at $n_z \simeq \pm 5.1, \pm 8.5, \ldots$.

It is in the nature of the exponential term of eq.(14) to generate a very broad nonlinear spectrum, a process controlled by the numerical filter. We studied the power loss ϵ_P as a function of E_0 and of the extent of the nonlinear region. In all cases, there is a value of E_0 for which the power loss is maximum, corresponding to maximum filamentation in the nonlinear region. For larger E_0 the density depression becomes so uniform in z as to produce less parallel nonlinear effects. With $\xi_1 = 1.0$ and $\xi_2 = 1.5$ we had $\epsilon_{P,max} = 0.15$, while for $\xi_1 = 2.0$ and $\xi_2 = 2.5$ we had $\epsilon_{P,max} = 0.27$. These large values point to the need of a more physical mechanism to control the nonlinearity. However, we expect the qualitative results of filamentation to remain valid.

7. Two Waveguide Array

A. Basic Excitation

We now consider the coupling of a two-waveguide array. The waveguides each have width b, and the fields in the apertures are given a relative phase ϕ. The fields are specified by:

$$E(\xi = 0, z) = \begin{cases} E_{01} e^{i\phi/2}, & 0 < z < b \\ E_{02} e^{-i\phi/2}, & -b < z < 0 \\ 0, & |z| > b \end{cases} \tag{31}$$

where $E_{01,2}$ is the total field amplitude in each aperture. The simplest case occurs when the excitation is symmetrical, with $\phi = 0$ or $\phi = \pi$. The reflection coefficients are then equal in right and left waveguides, and we have, assuming the same incident amplitude, $E_{01} = E_{02} \equiv E_0$. The Fourier transform of the excitation is:

$$\tilde{E}(\xi = 0, n_z) = E_0 \psi(n_z) \qquad \psi(n_z) = E_0 \frac{2}{\pi} \frac{\sin\left(\frac{1}{2} b n_z\right) \cos\left(\frac{1}{2}(b n_z - \phi)\right)}{n_z} \tag{32}$$

In this analysis we ignore higher order modes, and E_0 is the sum of the incident and reflected amplitudes E_i and E_r of the fundamental waveguide mode. Only E_i, which is imposed by the power source at the other end of the waveguide, is known beforehand.

The linear problem has been solved by Brambilla[18]. In his approach, electric and magnetic fields are matched at the mouths of the waveguides with those inside the plasma. In our simplified analysis the plasma acts as a simple load with complex admittance. The reflection coefficient is:

$$|R|^2 = \left|\frac{1 - Y_T}{1 + Y_T}\right|^2 \tag{33}$$

where Y_T is an effective plasma admittance, to be evaluated for $\phi = 0$ or $\phi = \pi$. It is given by:

$$Y_T = a^{1/3}\hat{Y}_T \qquad \hat{Y}_T = \frac{1}{E_0 e^{i\phi/2}}\frac{1}{b}\int_0^b H_{y,N}(\xi = 0, z)\,dz \tag{34}$$

where $H_{y,N}$ is the normalized magnetic field found analytically or numerically from:

$$\left(\frac{\partial^2}{\partial z^2} + 1\right) H_{y,N}(\xi, z) = i\frac{\partial E_z(\xi, z)}{\partial \xi} \tag{35}$$

When $a \gg 1$, which is almost always the case, $H_{y,N}(\xi = 0, z)$ is only weakly dependent on a. This simplification reduces considerably the numerical work needed to explore the coupling regimes.

An alternative expression for $\hat{Y}_T$ can be found by expressing eq.(34) in terms of Fourier transforms:

$$\hat{Y}_T = \frac{\pi}{b}\int_{-\infty}^{\infty} \hat{Y}_P(n_z)|\psi(n_z)|^2\,dn_z \qquad \hat{Y}_P(n_z) = -\frac{\tilde{H}_{y,N}(\xi = 0, n_z)}{\tilde{E}_z(\xi = 0, n_z)} \tag{36}$$

B. Linear Admittance and Numerical Method for the Nonlinear Admittance

In the linear steady-state we have:

$$\hat{Y}_P(n_z) = \frac{e^{i\frac{\pi}{6}}}{(n_z^2 - 1)^{2/3}}\frac{\mathrm{Ai}'(0)}{\mathrm{Ai}(0)} \tag{37}$$

where Ai is the Airy function, and where $(n_z^2 - 1)^{1/3} = e^{i\pi/3}|1 - n_z^2|^{1/3}$ for $|n_z| < 1$ and $(n_z^2 - 1)^{1/3} = e^{i2\pi/3}|n_z^2 - 1|^{1/3}$ for $|n_z| > 1$. The singularities in $\hat{Y}_P(n_z)$ come from the inversion of eq.(35), which, in Fourier space, has resonances at $n_z = \pm 1$. These resonances persist in the nonlinear calculation, because eq.(35) is unchanged.

Though the singularities in $\hat{Y}_P(n_z)$ are integrable, their presence may lead to numerical inaccuracy. In the plasma region, we have imposed periodic boundary conditions in z, at $z = \pm z_m$.

This is equivalent to solving a problem with the source repeated at regular intervals of $2z_m$. The periodicity requirement has the effect of singling out the Fourier components at $n_{zn} = n\pi/z_m = n\Delta n_z$, $n = 0, \pm 1, \pm 2, \ldots$. The numerical counterpart of eq.(36) is:

$$\hat{Y}_T^{\text{periodic}} = \frac{\pi}{b} \sum_{n=-\infty}^{\infty} \hat{Y}_P(n_{zn}) |\psi(n_{zn})|^2 \, \Delta n_z \tag{38}$$

where $\Delta n_z = \pi/z_m$. In the bulk of the Fourier spectrum, this sum may be a fair approximation to the integral of eq.(36). But near the resonances at $n_z = \pm 1$, the approximation becomes inaccurate. As a check we considered linear coupling and compared the results of eq.(36) with eq.(38) and with the results of the 2D integration. It is found that there is close agreement between the 2D results and eq.(38). This verifies the validity of the numerical scheme. On the other hand, $\hat{Y}_T^{\text{per}}$ differs considerably from $\hat{Y}_T$ in eq.(36) whenever the spectrum is sizeable near $n_z = \pm 1$. Furthermore, the convergence of $\hat{Y}_T^{\text{per}}$ to $\hat{Y}_T$ is very slow. Typically, to get a 5% accuracy, we need $\Delta n_z \simeq 0.02$. This requires $z_m \simeq 150$, and keeping $\Delta z = 0.15$, we need $N_z \simeq 2000$. This large number of mesh points is totally unfeasible in the 2D integration.

In view of the problems associated with the $n_z = \pm 1$ resonances, our approach will be the following. In the next section we propose a simpler model for the waveguide coupling. We verify this model by comparing $\hat{Y}_T^{\text{per}}$, eq.(38), with the results of the 2D computations. We then use the model to evaluate accurately the continuous integrals of eq.(36). This is now feasible because the numerical evaluation of $\hat{Y}(n_z)$ is much simpler with the 1D model. The final result for Y_T is our estimate of the "true", physical nonlinear plasma admittance.

C. Coupling Equation

We integrated numerically the wave equation for the excitation of the two-waveguide array. We considered a number of waveguide widths and the two phasings, $\phi = 0$ and π. For instance, results for the admittance $\hat{Y}_T$ are shown in figs.(9) for $\phi = 0$ and $b = 1.5$. We plot $\text{Re}(\hat{Y}_T)$ (crosses) and $\text{Im}(\hat{Y}_T)$ (squares) against E_0, the total field amplitude at the waveguide mouth. The general tendency is for $\hat{Y}_R$ and $\hat{Y}_I$ to decrease with increasing E_0, $\hat{Y}_I$ being less sensitive to increasing nonlinearity. The continuous curves are obtained from the model which we describe below.

In the previous sections, we examined large arrays of waveguides and found simplified models for the coupling. These models are valid provided the excitation spectrum is narrow, centered about one or two peaks in Fourier space, and is small in the vicinity of $n_z = \pm 1$. Clearly this is

not the case for the two-waveguide array.

Our approach here is to remain in real space and make a simplifying assumption about the nonlinear modification of the density profile. We assume (I) that the ξ-dependence of the density profile is the dominant effect in the loading of the waveguides, and (II) that this dependence can be approximated by assuming the density depression in front of the waveguides is infinite in z, and is created by a uniform field of amplitude E_0.

In accordance with this model, we first solve for the uniform density modification. Since $\partial/\partial z = 0$, eq.(14) reduces to:

$$\frac{d^2E_{dep}}{d\xi^2} - \xi \exp(-|E_{dep}|^2)E_{dep} = 0, \qquad E_{dep}(0) = E_0 \tag{39}$$

where "dep" stands for "depression". We then define a new density:

$$\hat{n}(\xi) = \xi \exp(-|E_{dep}(\xi)|^2) \tag{40}$$

which is obtained by solving eq.(39) numerically. We then solve a linear coupling problem, but one which incorporates the modified density. Eq.(14) becomes:

$$\frac{\partial^2 E}{\partial \xi^2} - \hat{n}(\xi)\left(\frac{\partial^2}{\partial z^2} + 1\right)E = 0 \tag{41}$$

Because the density term is z-independent, we can Fourier transform eq.(41) and obtain an ordinary differential equation:

$$\frac{d^2\tilde{E}(\xi, n_z)}{d\xi^2} + (n_z^2 - 1)\hat{n}(\xi)\tilde{E}(\xi, n_z) = 0 \tag{42}$$

For each value of n_z, eq.(42) must be solved numerically. However, this is a relatively simple procedure, and can be done for a very large number of Fourier modes, a number much larger than that allowed in the 2D integration. Thus, assuming the model is valid, we can hope to approximate much more closely the total plasma admittance.

We tested the coupling model for a number of waveguide widths ($0.5 < b < 2.0$) and for both $\phi = 0$ and π phasings. For instance, consider fig.(9). For comparison with the 2D results, plotted as discrete data points, the curves of figs.(9) were derived from the 1D model taking into account the effect of periodicity in the boundaries. Thus we evaluated $\hat{Y}_T^{\text{per}}$ from eq.(38), instead

of $\hat{Y}_T$ from eq.(36), and used 256 Fourier modes in the summation. In general, there is good agreement between 2D and 1D results for real part $\hat{Y}_R$, and lesser but qualitatively correct agreement with $\hat{Y}_I$.

Having gained confidence that the 1D model approximates the nonlinear coupling, we extend it to the "continuum" limit, by taking many more modes ($\gg$ 256) in the summation of eq.(38). Then we can compute the power reflection in the waveguides according to eq.(33). The incident field amplitude, E_i, is given by $E_i = \frac{1}{2}\left(1 + \alpha^{1/3}\hat{Y}_T\right)E_0$. The results for the reflection coefficient are shown in figs.(10), where $|R|^2$ is plotted parametrically against E_i for $b = 1.0$ and for density gradients $\alpha = 64, 540$. These values are representative of the ALCATOR-A and PETULA experiments. In the calculations, we took $\Delta n_z = 0.02$, with 2000 Fourier modes.

Figs.(10) allow for extremely large nonlinearity, $E_i = 40.0$. In fact, such large fields can never be attained. A convenient formula for estimating the normalized field amplitude is:

$$E_i = \frac{2.9}{f}\sqrt{\frac{S_i}{T_e + T_i}} \tag{43}$$

where a plane wave is assumed incident in the parallel plate waveguides. In eq.(43) S is in kW/cm^2, f is in GHz, and $T_{e,i}$ are in eV. Assuming rather extreme values $f = 0.5$ GHz, $T_e + T_i = 2$ eV and $S = 10$ kW/cm^2, we find a maximum E_i, $E_{i,max} \simeq 13.0$.

In the range $0 < E_i < 13.0$, the results of the coupling model show that nonlinear effects are more pronounced at weak gradients and are stronger for the narrower waveguides. This is not suprising. At weak gradients, the linear coupling is better because there is less mismatch between plasma and waveguides. The transmitted field amplitudes are larger and hence the nonlinearity is enhanced from the outset. Also, a narrow waveguide has a broader spectrum, and the shorter wavelengths excited by this spectrum are more affected by the nonlinear density profile. The nonlinear density modification is of finite extent in ξ, and more transparent to long wavelengths.

D. Numerical Results for the Spectrum of the Two-Waveguide Array

In figs.(11) are shown results for an excitation of two waveguides in phase, $\phi = 0$, with each waveguide of width $b = 1.0$. In our model we neglect the existence of a septum, so that this excitation looks like a single waveguide of width $b = 2.0$. Three regimes can be discerned as a function of increasing nonlinearity:

(1) Weak Nonlinearity : For $E_0 < 1$ modifications on fields and spectra are weak. In real

space, there is weak focusing of the fields near the source. There is some enhancement of the side lobes of the Fourier spectrum at the exit plane, but the spectrum retains its original shape (figs.(11a, 12a)).

(2) Moderate Nonlinearity : In the range $1 < E_0 < 2$ a sharp transition of nonlinear effects occurs, and this leads to strong modification of the fields. In real space, we see the formation of a sharply peaked "ridge" in front of the waveguide which extends some distance into the plasma (fig.(11b)). Because of this region of strong focusing, the Fourier spectrum is broadened and shifted (fig.(12b)). In the range $|n_z| > 1$, some of the lower n_z are "depleted" to larger values. As E_0 is increased, more ridges form on the edges of the field profile.

(3) Large Nonlinearity : For $E_0 > 2$, we see a "tunnelling effect" effect becoming dominant (fig.(11c)). Right in front of the source, a large density trough forms, and in this trough the fields are fairly smooth. It is only some distance into the plasma that sharp ridges form in the field profile, and the nonlinear effects on the spectrum are reduced (fig.(12c)). With a nonlinear region of finite length, and sufficiently large E_0, the region of strong self-focusing may disappear completely.

In discussing the power spectra obtained for the examples discussed above, we look at the power in three regions of n_z space: (I) $1.0 < n_z < 2.0$, (II) $2.0 < n_z < 6.0$ and (III) $6.0 < n_z < \infty$. P_I and P_{II} are calculated by summing Fourier components in the power spectrum. P_{III} is defined as the power dissipated in the numerical filter, which is simply $P_{TOT} - P_I - P_{II}$, where P_{TOT} is the total power coupled at the source. Results are shown in fig.(13a). We see that for $E_0 \ll 1$ most of the power coupled at the exit plane lies in region (I), that is in $n_z < 2.0$. As E_0 increases, there appears to be a fairly sharp threshold for dumping power into region (II), and to a lesser extent into region (III). This corresponds to the onset of strong self-focusing of the fields. Finally, at large field amplitudes, region (II) is depleted again, and most power at large n_z is in region (III). Presumably, in this extreme regime it is in the sharp sides of the density trough that most power is dissipated. Inside the trough, the fields are smooth and dissipate little power.

We repeated the numerical runs described above for the waveguides out of phase, $\phi = \pi$. The qualitative discussion given above applies to this case as well. In fig.(13b) we show how power is transferred between the three regions in n_z space. Here there is no intermediate regime where power from region (I) ($1.0 < n_z < 2.0$) is dumped into region (II) ($2.0 < n_z < 6.0$). Rather, power from (I) and (II) is transferred directly to region (III).

In comparing figs.(13a) ($\phi = 0$) and (13b) ($\phi = \pi$) we note that at the largest field amplitude roughly as much power ends up in region (III) in both cases, with region (II) depleted relative to the other two regions. However, we cannot conclude that both phasings will produce the same power spectrum (and hence the same heating effects inside the plasma). First, because as discussed above the power transfer picture of figs.(13) is at best qualitative, and second, because the initial total power coupled at the source may be quite different because of the different reflection coefficients.

8. Comparison with Experiment

A. Reflection Coefficient

In the PETULA experiment[19,20], twin waveguides radiated up to 1 MW at a frequency of 1.25 GHz. Two array designs were used, one with total area of 117 cm^2 (3.55 cm $\times$ 16.5 cm apertures), the other with an area of 40 cm^2(1.8 cm $\times$ 11 cm apertures). In both cases, the maximum incident power was about 10 kW/cm^2. Experimental results for the reflection coefficient are the following. For the 117 cm^2 Grill, there is a strong reduction of $|R|^2$ in the range $2.6\ kW/cm^2 < P < 6.0\ kW/cm^2$. This occurs for both waveguide phasings. For the 40 cm^2 Grill, $|R|^2$ is fairly constant for $\phi = 0$, and increases steadily for $\phi = \pi$.

We apply the 1D model of eqs.(39,40,41) to obtain theoretical values for the reflection coefficient. The normalized waveguide widths are $b = 0.92$ for the 117 cm^2 array and $b = 0.64$ for the 40 cm^2 array. We estimate the density gradient by assuming that the low-power regime is predicted by Brambilla theory. For linear experimental and theoretical values to concur, we find that we need $\alpha \simeq 500$. We estimate the edge temperature by taking $T_e = T_i = 1$ eV. The results of the 1D model are shown in figs.(14).

In the case of the 117 cm^2 Grill, there is little agreement between model and experiment. The salient feature of the experimental results, the decrease of $|R|^2$ for both phasings, is not seen. For the 40 cm^2 Grill, there is qualitative agreement in the results. The model predicts successfully that the $\phi = \pi$ phasing is more sensitive to nonlinearity and that $|R|^2$ should increase for this phasing. We emphasize that because of uncertainty in the edge temperature, the horizontal scales of figs.(14) could change considerably. This may better or worsen the fit of the theoretical predictions.

In the ALCATOR-A[21,22] experiment, two waveguides of dimensions 1.3 cm $\times$ 8.1 cm, radiated up to 90 kW of RF at 2.45 GHz. The peak power density was lower than in the PETULA

experiment, $P_{i,max} \simeq 5$ kW/cm^2. In this experiment, nonlinear effects were not seen in the reflection coefficient which retained its linear phase dependence at all incident powers.

What is the prediction of the 1D model, eqs.(39-41)? The normalized waveguide width is $b = 0.66$, and the best fit to Brambilla results at low power obtains for $a \simeq 60$. We assume $T_e = T_i = 3$ eV, roughly the values observed in probe measurements[15]. The results are shown in fig.(15). In the range $0 < P_i < 5$ kW/cm^2, the theory predicts only small changes in reflectivity.

In the experiment performed on the JFT-2 Tokamak[23], an array of four waveguides handled up to 300 kW of incident power at a frequency of 750 MHz. A strong dependence of the coupling on incident power was observed, with $|R|^2$ decreasing with increasing power at all phasings of the array. Above about 50 kW, the effect saturated, with reflectivity becoming uniformly small, $|R|^2 < 0.1$.

In an attempt to explain these results by ponderomotive effects, we use all the 1D coupling models derived above. The waveguides have dimensions 1.4 cm $\times$ 29.0 cm. In normalized units, the waveguide width is $b = 0.22$. The gradient parameter is determined once again by a fit of Brambilla theory to the low-power data. It is found to be $a = 2.7 \times 10^4$. The power density is roughly $S = 0.27$ kW/cm^2 at 50 kW and $S = 1.7$ kW/cm^2 at 300 kW. We assume edge temperatures $T_e = T_i = 1$ eV.

We consider separately the three phasings, $\phi = 0, \frac{\pi}{2}, \pi$. We determine $|R|^2$ for $\phi = 0$ from eqs.(39,40,41). For $\phi = \frac{\pi}{2}$ we use the travelling wave model, eq.(24), and for $\phi = \pi$ we use the standing wave model, eq.(29). The results are shown in fig.(16). The theoretical predictions are not consistent with the experiment. According to theory, $|R|^2$ should increase for $\phi = \frac{\pi}{2}, \pi$, and decrease very little for $\phi = 0$, while in the experiment $|R|^2$ decreases markedly for all phasings, $\phi = \frac{\pi}{2}, \pi$ and 0.

B. Spectrum

We saw that filamentation of the fields and broadening of the power spectrum occurred when $e^2|E_z|^2/4m_e\omega^2(T_e + T_i) \simeq 1$, a condition well reached if we make the same assumptions about edge temperatures as above. However, there is no strong evidence for a nonlinear upshift of the spectrum. In JFT-2 the excited spectrum appeared to be linear. In ALCATOR-A, an upshift was deduced, but this upshift is constant over a broad range of incident power. This suggest rather that a linear mechanism is in cause[24].

11. Conclusions

We analysed the importance of ponderomotive effects in the coupling of a number of waveguide excitations. Both numerical and semi-analytic methods were used and three simplified models were derived to cover a large number of cases.

We first studied the coupling of a large array, which has narrow peaks in its Fourier spectrum. Both travelling wave ($\phi = \frac{\pi}{2}$) and standing wave ($\phi = \pi$) excitations were considered. We derived a model to predict power coupled by the standing wave.

The power spectrum of the travelling wave is broadened and downshifted by nonlinear effects, but remains unidirectional. The power spectrum of the standing wave is more sensitive to nonlinearity. Because of harmonic generation in Fourier space, it may be considerably upshifted. In real space, the fields undergo filamentation.

We next studied small arrays and derived a coupling theory for the two waveguide array. The theory predicts that substantial changes in reflectivity can occur, but these require weak density gradients or large power densities. Narrow waveguides are also more sensitive to nonlinear effects. The new coupling theory differs substantially from that of Chan and Chiu[7]. It predicts coupling of excitations with power near $n_z \simeq 1$, a regime where the other theory breaks down.

The power spectra of the small array can be considerably broadened by nonlinearity. This again corresponds to filamentation in real space. The results suggest that the power spectra for $\phi = 0$ and $\phi = \pi$ may be made similar by nonlinear effects, but limitations on the numerical scheme did not permit quantitative estimates.

Comparison of the coupling theory with experimental data was inconclusive. This negative result is mitigated by the fact that other effects not included in the theory (low frequency fluctuations, parametric excitations) might be responsible for suppressing the ponderomotive effects. This would not preclude regimes where the ponderomotive effects might be important.

A major limitation of the numerical scheme is that it requires artificial dissipation to control nonlinear instability. A suggestion for future work is to replace the dissipation by a physical mechanism, in the form of thermal dispersion in the high frequency equation. This would complicate the physics but yield more satisfactory solutions.

A second suggestion for extending the present work is to retain the low-frequency dynamics and allow for coupling to ion-acoustic waves. This is the approach followed by Fukuyama et al.[12].

It is a numerically more demanding problem but allows for richer physics.

Acknowledgments

I wish to thank Prof. A. Bers for his guidance in the present work. My thanks also go to Drs. K. C. Ko and V. Krapchev who have collaborated on several aspects of this problem.

This work was supported by United States Departement of Energy Contract DE-AC02-78ET-51013 and National Science Foundation Grant ENG 79-07047.

Appendix A. Weak Nonlinearity

The Nonlinear Klein-Gordon Equation includes electromagnetic effects, and allows for the strong interaction of both resonance cones. To see the connection with other nonlinear equations, we consider the region beyond the limiter shadow where the temperature is much larger. In this region the nonlinearity is weak and can be considered a perturbation to linear propagation. We include thermal dispersion by adding higher order derivatives corresponding to higher order terms in the linear dispersion relation[25]. With the exponential nonlinearity expanded we have:

$$\frac{\partial^2 E}{\partial \xi^2} - \left(\frac{\partial^2}{\partial z^2} + 1\right)E + \left(\frac{\partial^2}{\partial z^2} + 1\right)(|E|^2 E) + \delta_1 \frac{\partial^4 E}{\partial z^4} + \delta_2 \frac{\partial^4 E}{\partial z^2 \partial \xi^2} + \delta_3 \frac{\partial^4 E}{\partial \xi^4} = 0 \qquad (44)$$

For simplicity we assume a homogeneous plasma, $A_0(x) = \text{constant} \gg 1$. The new coordinate is $\xi = A_0^{1/2} x$. The coefficients δ_j are given by: $\delta_1 = 3\left(\frac{v_{te}}{c}\right)^2 + 3\frac{m_e}{m_i}\left(\frac{v_{ti}}{c}\right)^2, \delta_2 = -\frac{\omega_{pe}^2}{\Omega_e^2}\left(\frac{v_{te}}{c}\right)^2 + 6\frac{\omega_{pi}^2}{\omega^2}\left(\frac{v_{ti}}{c}\right)^2, \delta_3 = \frac{3}{4}\frac{\omega_{pe}^4}{\Omega_e^4}\left(\frac{v_{te}}{c}\right)^2 + 3\frac{\omega_{pe}^2}{\omega^2}\frac{\omega_{pi}^2}{\omega^2}\left(\frac{v_{ti}}{c}\right)^2$, where $v_{ts} = (T_s/m_s)^{1/2}$.

In the outer plasma layers we have $\omega_{pi}(x) \ll \omega$ and $\omega_{pe}(x) \ll \Omega_e$. With these conditions we find $\delta_3 \ll \delta_2 \ll \delta_1 \simeq 3\left(\frac{v_{te}}{c}\right)^2$, and we may neglect terms in $\delta_{2,3}$.

If we assume the excitation spectrum at the edge is narrow, and centered about $n_z = n_{z0}$, we can derive a nonlinear Schoedinger equation (NLSE) from eq.(44). This is done by a reductive treatment of the equation[26]. The form of the solution is:

$$E(\xi, z) = e^{in_{z0}z} e^{ik_0\xi} \tilde{E}(\xi, z) \qquad (45)$$

where $\tilde{E}(\xi, z)$ is a slowly-varying function of ξ and z and where n_{z0} is imposed by the source. To lowest order, $k_0 = -(n_{z0}^2 - 1)^{1/2}$. This slow dependence is further broken up by writing:

$$\tilde{E}(\xi, z) = \hat{E}(\xi, \varsigma) \qquad \varsigma = z - \frac{n_{z0}}{(n_{z0}^2 - 1)^{1/2}}\xi \tag{46}$$

where ς denotes deviation from the central ray and ξ measures the distance over which there are nonlinear and linear dispersive effects. We obtain the NLSE:

$$i\frac{\partial \hat{E}}{\partial \xi} + \left(\frac{3n_{z0}^2}{(n_{z0}^2 - 1)^{1/2}}\delta_1 - \frac{1}{2(n_{z0}^2 - 1)^{3/2}}\right)\frac{\partial^2 \hat{E}}{\partial \varsigma^2} + \frac{1}{2}(n_{z0}^2 - 1)^{1/2}|E|^2\hat{E} = 0 \tag{47}$$

This equation, but without thermal dispersion, has been derived by Krapchev and Bers[9]. Eq.(20) shows that electromagnetic dispersion opposes thermal effects. The equation is modulationally unstable when the coefficients of the second-order derivative and of the nonlinear term are of the same sign[27]. By inspection, we see that this requires:

$$n_{z0} > n_{0c} = 0.67\delta^{-1/4} = 0.5\left(\frac{c}{v_{te}}\right)^{1/2} \tag{48}$$

For instance, with $T_e \simeq 100\,\mathrm{eV}$, we find $n_{0c} \simeq 5$, which is not small. Thus electromagnetic dispersion can inhibit filamentation over a large part of the spectrum, at least in the outer plasma layers.

If we consider perturbations of a single resonance cone, but do not assume a narrow spectrum, we can derive a CMKdV equation with electromagnetic effects. In eq.(44), we take $E(\xi, z) = \hat{E}(\xi, z - \xi) = \hat{E}(\xi, \varsigma)$, where ς measures deviation from the resonance cone and ξ is a weak dependency which scales as the nonlinearity and thermal dispersion. Expanding eq.(44) with $\partial/\partial\varsigma \gg 1$, we obtain:

$$\frac{\partial E}{\partial \xi} - \frac{\delta_1}{2}\frac{\partial^3 E}{\partial \varsigma^3} - \frac{1}{2}\frac{\partial}{\partial \varsigma}(|E|^2 E) + \frac{1}{2}\int_{-\infty}^{\varsigma} E\, d\varsigma' = 0 \tag{49}$$

where we assume $E(\xi, \varsigma = -\infty) = 0$. This is an equation analysed by Hsu and Kuehl[28]. They have found that the electromagnetic term tends to suppress filamentation, a conclusion consistent with the results obtained from the NLSE.

Appendix B. Numerical Method for the Nonlinear Equation

We solve eq.(18) with zero field initial conditions. The fields are imposed at $\xi = 0$, starting with zero amplitude, and are ramped in a few time steps to a constant value. We use a finite difference, implicit scheme to advance the numerical analog of eq.(18). The computational region is a rectangle, with dimensions $0 < \xi < \xi_m$ and $-z_m < z < z_m$, and this region is covered by a grid of dimensions $N_\xi \times N_z$. At $\xi = \xi_m$, a numerical radiation boundary condition is implemented[29]. This condition requires linear propagation and is the reason for introducing a transition to the linear region. At the boundaries $z = \pm z_m$, periodic boundary conditions are imposed. At each time step we invert a very large but very sparse matrix by relaxation.

The usual mesh size is $N_\xi \times N_z = 27 \times 256$, and we take $\Delta\xi = 0.135$ and $\Delta z = 0.15$, for which $\xi_m = 3.5$ and $z_m = 19.5$. This is consistent with the ALCATOR-A parameters discussed above, for which the extent in ξ is $\delta\xi = a^{1/3}\delta x = 2.05$. We made this region a little bigger to allow for the linear transition region, and took $\xi_m = 3.5$. The value of z_m is large enough to accomodate most of the dispersion in propagation across the coupling region. A typical time step is $\Delta\tau = 0.25$ and roughly 150 time steps are necessary to reach the steady-state after the excitation is turned on. As for the depth of the nonlinear region, in the computer runs discussed below we took $\xi_1 = 2.0$ and $\xi_2 = 2.5$.

To avoid aliasing problems with the nonlinearity, a digital filter was used[30]. This filter introduces artificial dissipation in $|n_z| > n_1$. For $|n_z| < n_1$, the dissipation is negligible. The cutoff of the filter is given roughly by $n_1 = 0.3\, n_{z,max} = 0.3\frac{\pi}{\Delta z}$. Because of the filter, we are not really solving the finite-difference approximation of eq.(18), but the finite-difference approximation of eq.(18) to which a dissipative term has been added. The "harm" done to the spectrum can be gauged by the total power lost as waves propagate from the source to the far boundary. The fractional power loss is:

$$\epsilon_P \equiv \left| \frac{P_R(0) - P_R(\xi_{max})}{P_R(0)} \right| \tag{50}$$

and we require that ϵ_P be small for a solution to be an acceptable approximation to the solution of the dissipationless problem.

In practice, we have found that in many cases of nonlinear propagation ϵ_P is large ($\epsilon_P \simeq 0.3 - 0.4$) and it is hard to reduce this fractional power loss. For instance, increasing the mesh

resolution, say by going to a 54×512 mesh with $\Delta\xi = 0.0675$ and $\Delta z = 0.075$ does not help because the spectrum has become prohibitively large, even for the broader Fourier space afforded by the finer mesh. This situation is due to the filamentation of the fields in real space and points out a basic limitation of the numerical scheme. Because we have neglected thermal dispersion in the high frequency equation, there is no physical mechanism for balancing the strong self-focusing effects. It is the filter which keeps the spectrum from "running away", at the price of dissipating energy. This limits the physical validity of the power spectra obtained inside the plasma, whenever ϵ_P is "large", say $\epsilon_P > 0.1$.

On the other hand, it is found empirically that the numerical value of the plasma admittance at the waveguide mouths is not sensitive to the mesh size or to the amount of dissipation. This is because filamentation does not occur immediately in front of the waveguide apertures. In the region which determines the waveguide loading, propagation is adequately handled by the numerical scheme.

References

[1] BERS, A., Bull. Amer. Phys. Soc., 23 (1978) 765.

[2] KARNEY, C. F. F. K., Phys. Fluids, 24 (1981) 127.

[3] LECLERT, G., KARNEY, C. F. F., BERS, A., KAUP, D., Phys. Fluids, 22(1979).

[4] MORALES, G., LEE, Y., Phys. Rev. Lett., 35 (1975) 930.

[5] KARNEY, C. F. F., SEN, A., CHU, F. Y. F., Phys. Fluids, 22 (1979) 940.

[6] MORALES, G., Phys. Fluids, 20 (1977) 1164.

[7] CHAN, V., CHIU, S., Phys. Fluids, 22 (1979) 1724.

[8] FUKUYAMA, A., MORISHITA, T., FURUTANI, Y., Plasma Phys., 22 (1980) 565.

[9] KRAPCHEV, V., BERS, A., Proc. Third Topical Conf. on RF Plasma Heating, California Institute of Technology, Pasadena, California, Jan 11-13, 1978, G5-1.

[10] KRAPCHEV, V., THEILHABER, K., KO, K., BERS, A., Phys. Rev. Lett., 46 (1981) 1398.

[11] KO, K. C., Annual Controlled Fusion Theory Conference, April 8-10, 1981, Austin, Texas, 2B31.

[12] FUKUYAMA, A., Fourth Topical Conference on RF Heating in Plasma, February 9-10, 1981, Fusion Research Center, University of Texas, Austin, Texas, C13.

[13] VALEO, E., Bull. Amer. Phys. Soc., **25**, 8 (1980).

[14] THEILHABER, K. S., *Nonlinear Coupling to Lower Hybrid Waves in a Tokamak Plasma*, Doctoral Thesis, Massachusetts Institute of Technology, Cambridge, Massachusetts.

[15] SCATURRO, L., S., KUSSE, B., Nucl. Fusion, **18** (1978).

[16] ALLIS, W. P., BUCHSBAUM, S. J., BERS, A., *Waves in Anisotropic Plasmas*, MIT Press, Cambridge, Massachusetts, USA, 1963.

[17] CARY, J. R., KAUFMAN, A. N., Phys. Rev. Lett. **39** (1977) 403.

[18] BRAMBILLA, M., Nucl. Fusion, **16** (1976) 47.

[19] SINGH, C., BRIAND, P., DUPAS, L., *Idem.*

[20] BRIFFOD, G., WEGA and PETULA TEAMS, International Conference on Plasma Physics, IAEA, Brussels, July 980.

[21] SCHUSS, J. J., FAIRFAX, S., KUSSE, B., PARKER, R. R., PORKOLAB, M., et al., Phys. Rev. Lett., **43** (1979) 274.

[22] SURKO, C. M., SLUSHER, R. E., Phys. Rev. Lett., **43** (1979) 1016.

[23] NAGASHIMA, T., FUJISAWA, N., Proc. of the Joint Varenna-Grenoble International Symposium on Heating in Toroidal Plasmas, July 3-7, 1978, p.281, vol. 2.

[24] BONOLI, P. T., OTT, E.,Phys. Rev. Lett., **46** (1981) 424.

[25] SEN, A., KARNEY, C. F. F., JOHNSTON, G. L., BERS, A., Nucl. Fusion, **18** (1978) 171.

[26] TANIUTI, T., YAJIMA, N., J. of Math. Phys., **10** (1969).

[27] BUTI, B., Phys. Rev. Lett., **38** (1977) 498.

[28] HSU, P., KUEHL, H. H., Bull. Amer. Phys. Soc., 25, 8 (1980).

[29] ENGQUIST, B., MAJDA, A., Comm. Pure and Applied Math., 32 (1979) 313.

[30] SHAPIRO, R., Rev. Geophysics and Space Physics, 8 (1970) 359.

Figure Captions

1. Slab model of the coupling geometry.

2. Field amplitudes for the travelling wave excitation, eq.(19) ($n_{z0} = 2.0, z_0 = 4.0$, $\xi_1 = 2.0, \xi_2 = 2.5$): (a) $E_0 = 0.01$, (b) $E_0 = 3.0$.

3. Power spectra for the travelling wave excitation ($n_{z0} = 2.0, z_0 = 4.0, \xi_1 = 2.0$, $\xi_2 = 2.5$): (a) $E_0 = 0.01$, (b) $E_0 = 3.0$. The vertical scale is arbitrary, and the curves are normalized to the same peak amplitude.

4. Complex power coupled for the travelling wave excitation ($2\alpha^{-1/3}P(0)$ for $n_{z0} = 2.0, z_0 = 4.0, \xi_1 = 2.0, \xi_2 = 2.5$): Comparison of the two coupling models. Re(P): crosses (2D) and full line (1D); Im(P): squares (2D) and dashed line (1D).

5. Complex power coupled for the standing wave excitation ($2\alpha^{-1/3}P(0)$ for $n_{z0} = 1.7, z_0 = 6.0, \xi_1 = 1.5, \xi_2 = 2.0$): comparison of two coupling models. Re(P): crosses (2D) and full line (1D); Im(P): squares (2D) and dashed line (1D).

6. Reflection coefficient for the standing wave array (large array with $\phi = \pi$ phasing); $Q = \alpha^{1/3}/(n_{z0}^2 - 1)^{2/3}$.

7. Field amplitudes for the standing wave excitation, eq.(25) ($n_{z0} = 1.7, z_0 = 6.0$, $\xi_1 = 1.5, \xi_2 = 2.0$): (a) $E_0 = 1.0$, linear propagation, (b) $E_0 = 1.5$.

8. Fourier spectra at $\xi = 3.5$ for the standing wave excitation ($n_{z0} = 1.7, z_0 = 6.0$, $\xi_1 = 1.5, \xi_2 = 2.0$): (a) $E_0 = 1.0$, linear propagation, (b) $E_0 = 1.5$.

9. Total plasma admittance for a two-waveguide array ($b = 1.5, \phi = 0$): comparison of the 2D model (discrete points) with the 1D model (curves).

10. Reflection coefficient for a two waveguide array, as predicted by the 1D model ($b = 1.0, \phi = 0$ or π): (a) $\alpha = 64$, (b) $\alpha = 540$.

11. Field amplitudes for the two waveguide excitation, eq.(31) ($b = 1.5, \phi = 0$, $\xi_1 = 2.0, \xi_2 = 2.5$): (a) $E_0 = 0.01$, (b) $E_0 = 1.414$, (c) $E_0 = 3.0$.

12. Power spectra at $\xi = 3.5$ for the two waveguide excitation, eq.(31) ($b = 1.5$, $\phi = 0$, $\xi_1 = 2.0$, $\xi_2 = 2.5$): (a) $E_0 = 1.0$, linear propagation, $\beta(x) \equiv 0$, (b) $E_0 = 1.414$, (c) $E_0 = 3.0$.

13. Power transfer results for the two waveguide excitation ($b = 1.0$, $\xi_1 = 2.0$, $\xi_2 = 2.5$); $P_I = P(1 < |n_z| < 2)$, $P_{II} = P(2 < |n_z| < 6)$, $P_{III} = P$(power dissipated in the filter, $|n_z| > 6$): (a) $\phi = 0$, (b) $\phi = \pi$.

14. Reflection coefficients for PETULA (two waveguides): (a) 117 cm^2 Grill, $b = 0.92$, $a = 500$, $T_e = T_i = 1$ eV, (b) 40 cm^2 Grill, $b = 0.64$, $a = 500$, $T_e = T_i = 1$ eV.

15. Reflection coefficients for ALCATOR-A (two waveguides): $b = 0.66$, $a = 60$, $T_e = T_i = 3$ eV.

16. Reflection coefficients for JFT-2 (four waveguides): $b = 0.22$, $a = 2.7 \times 10^4$, $T_e = T_i = 1$ eV.

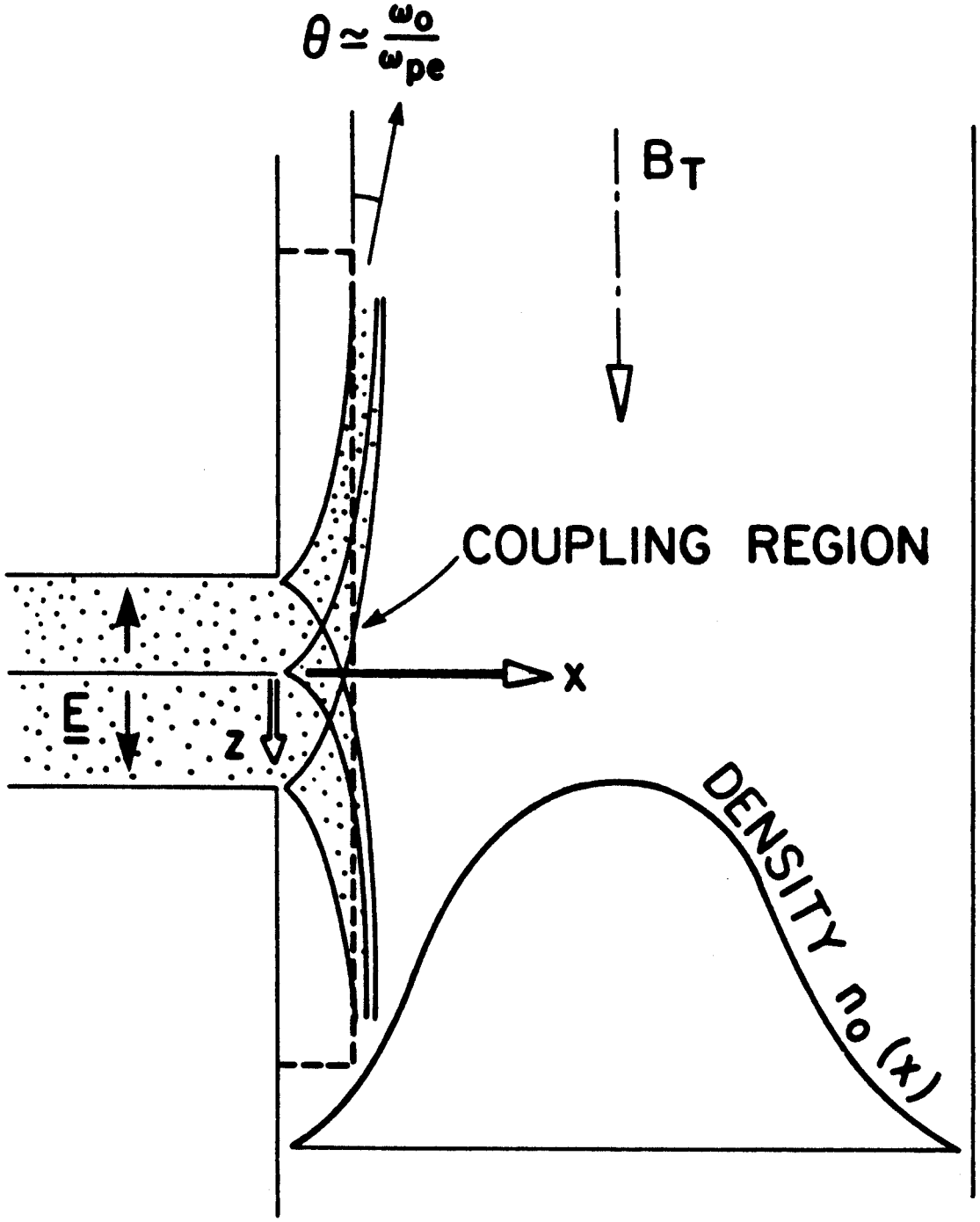
$\theta \simeq \frac{\omega_o}{\omega_{pe}}$
B_T
COUPLING REGION
x
E
z
DENSITY $n_o(x)$

FIG.(1)

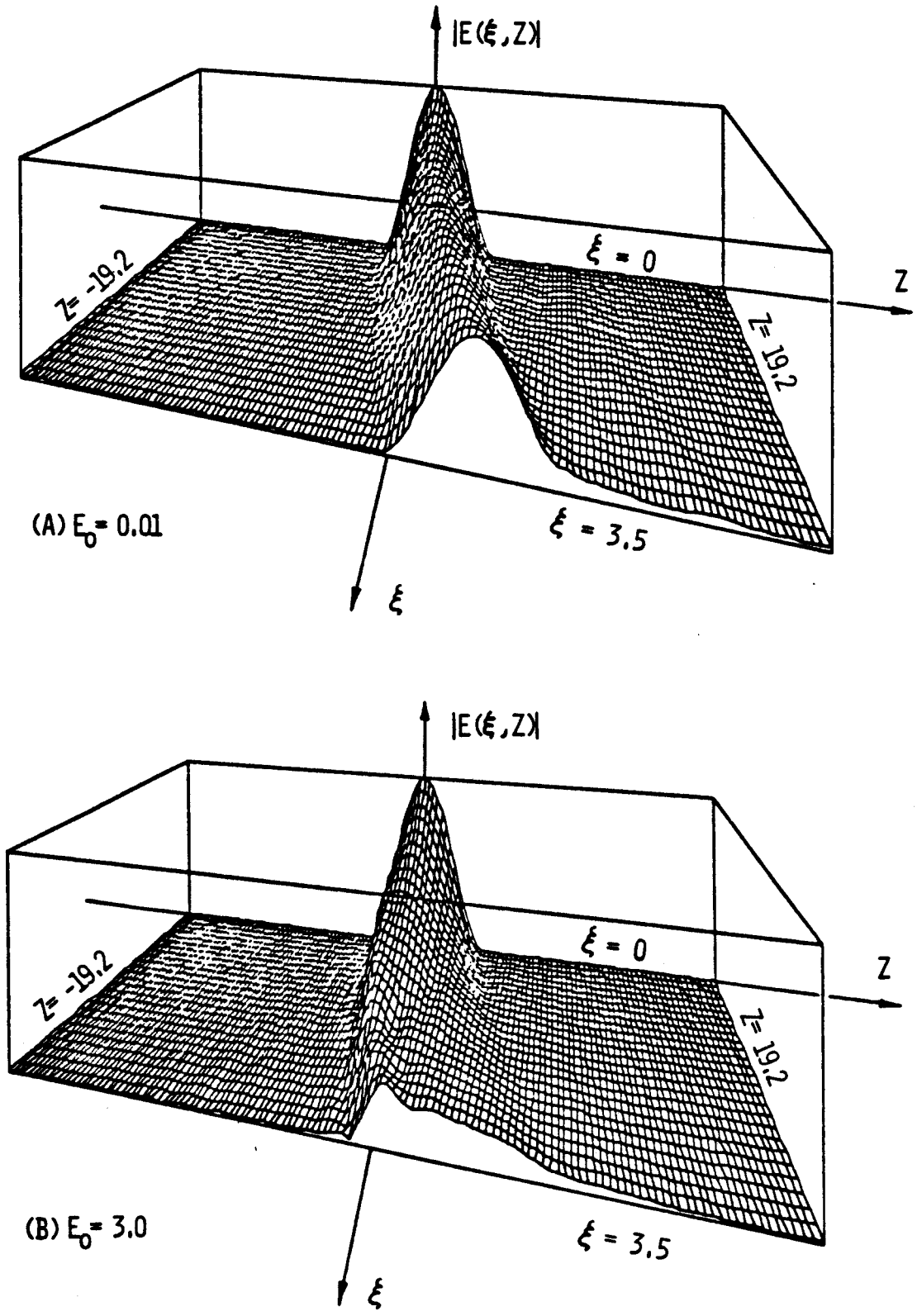

FIG. (2)

FIG.(2)

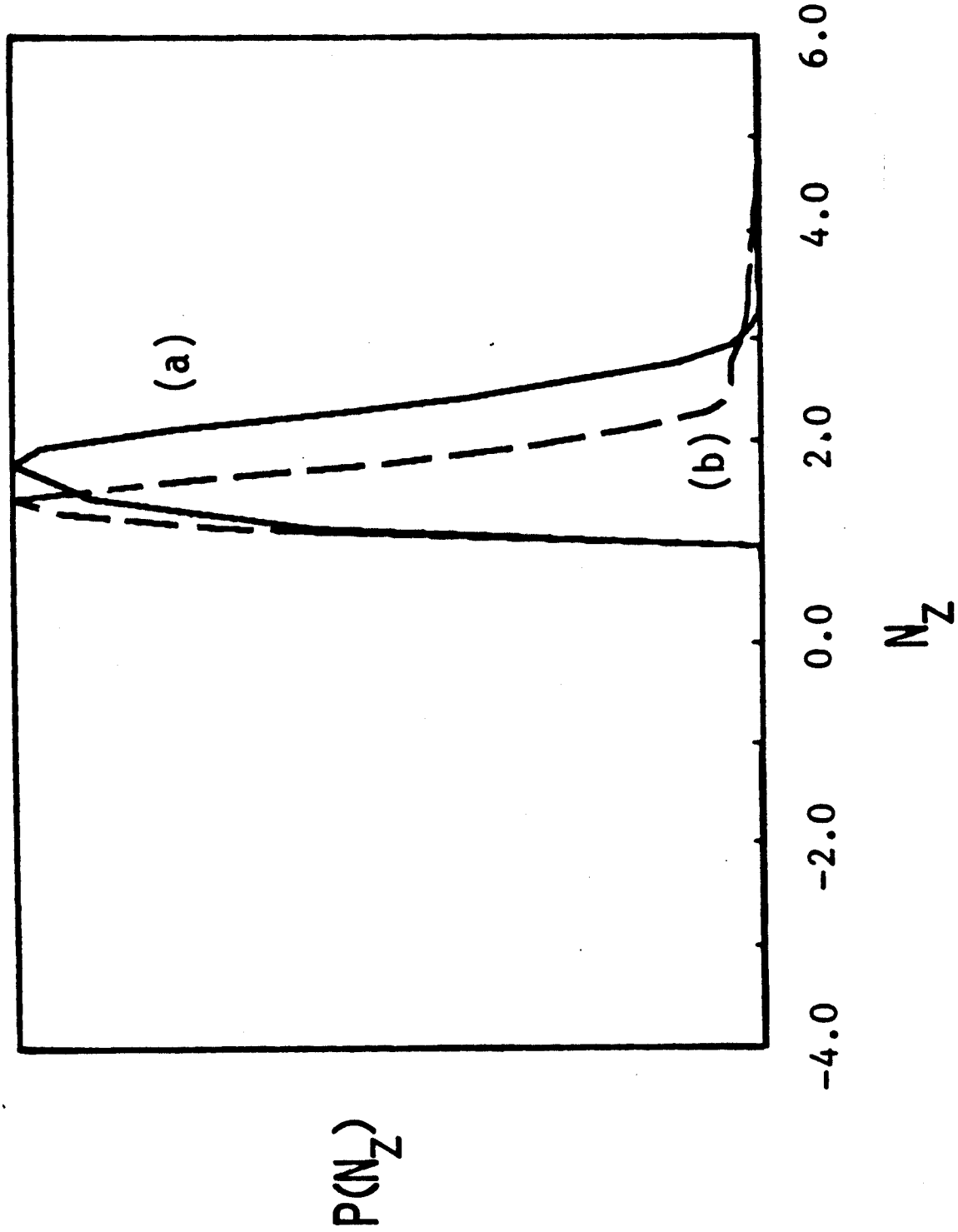

FIG.(3)

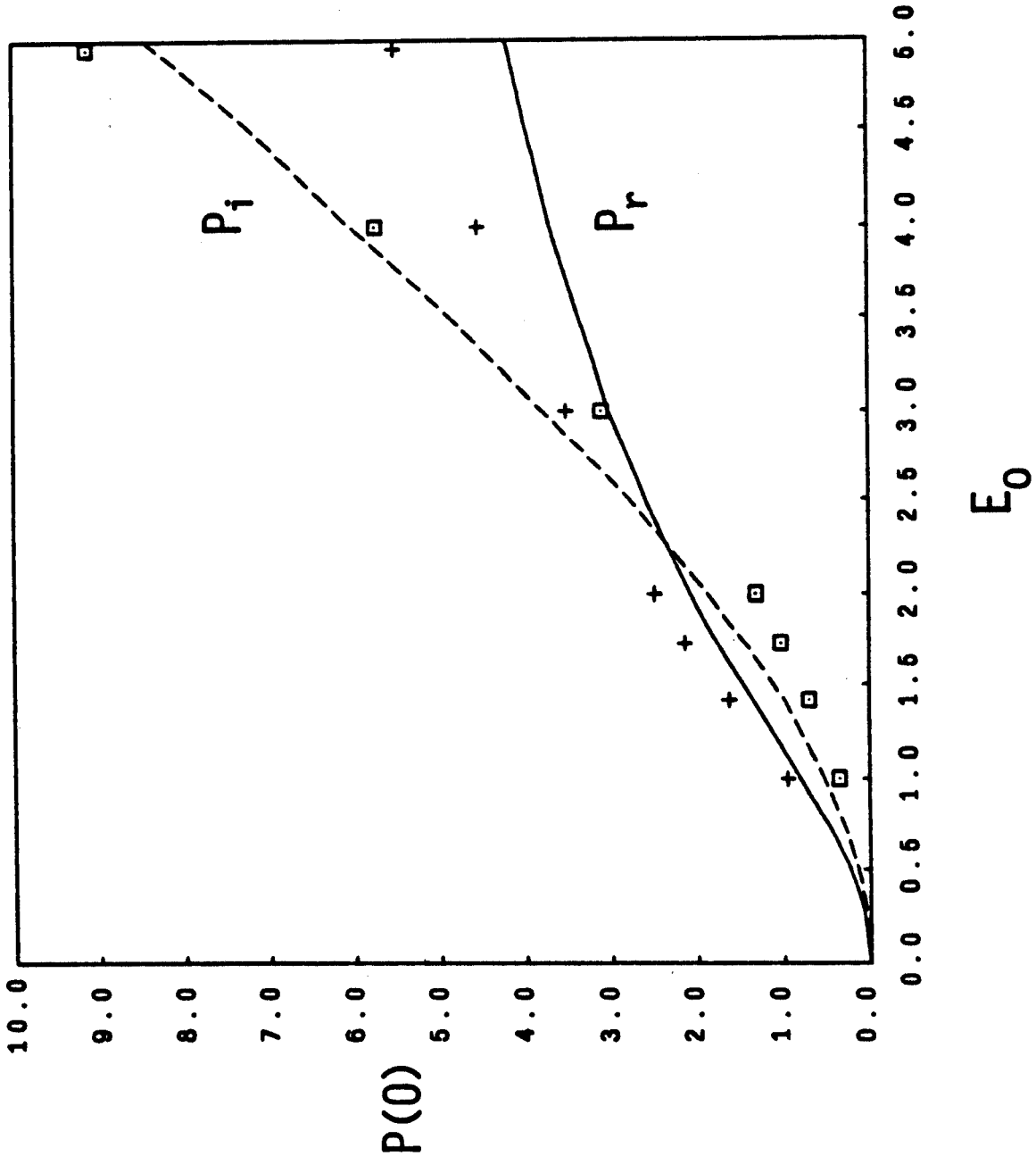
P_i
P_r
P(0)
E_0
10.0
9.0
8.0
7.0
6.0
5.0
4.0
3.0
2.0
1.0
0.0
0.0
0.6
1.0
1.6
2.0
2.5
3.0
3.5
4.0
4.5
6.0

FIG.(4)

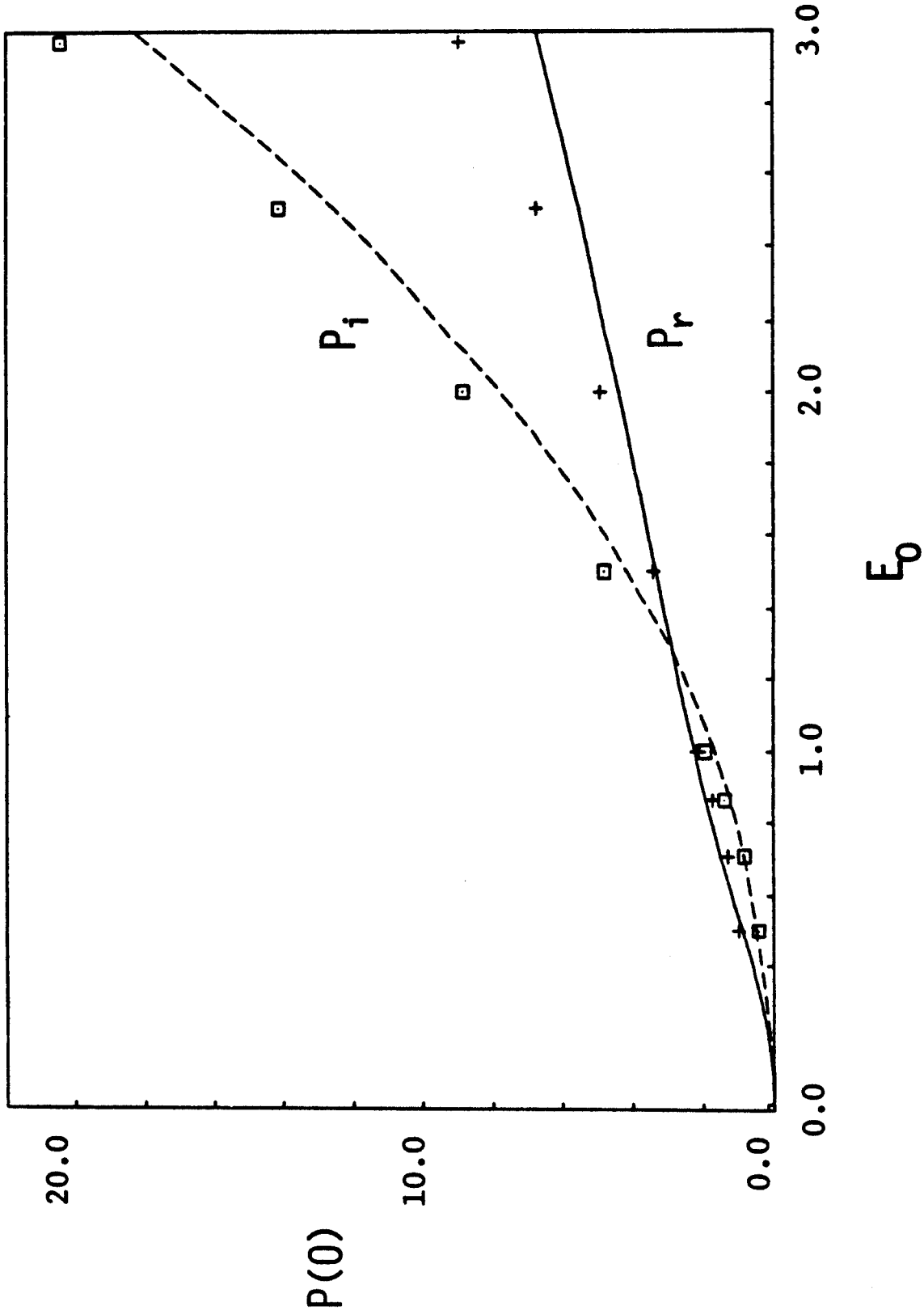

FIG.(5)

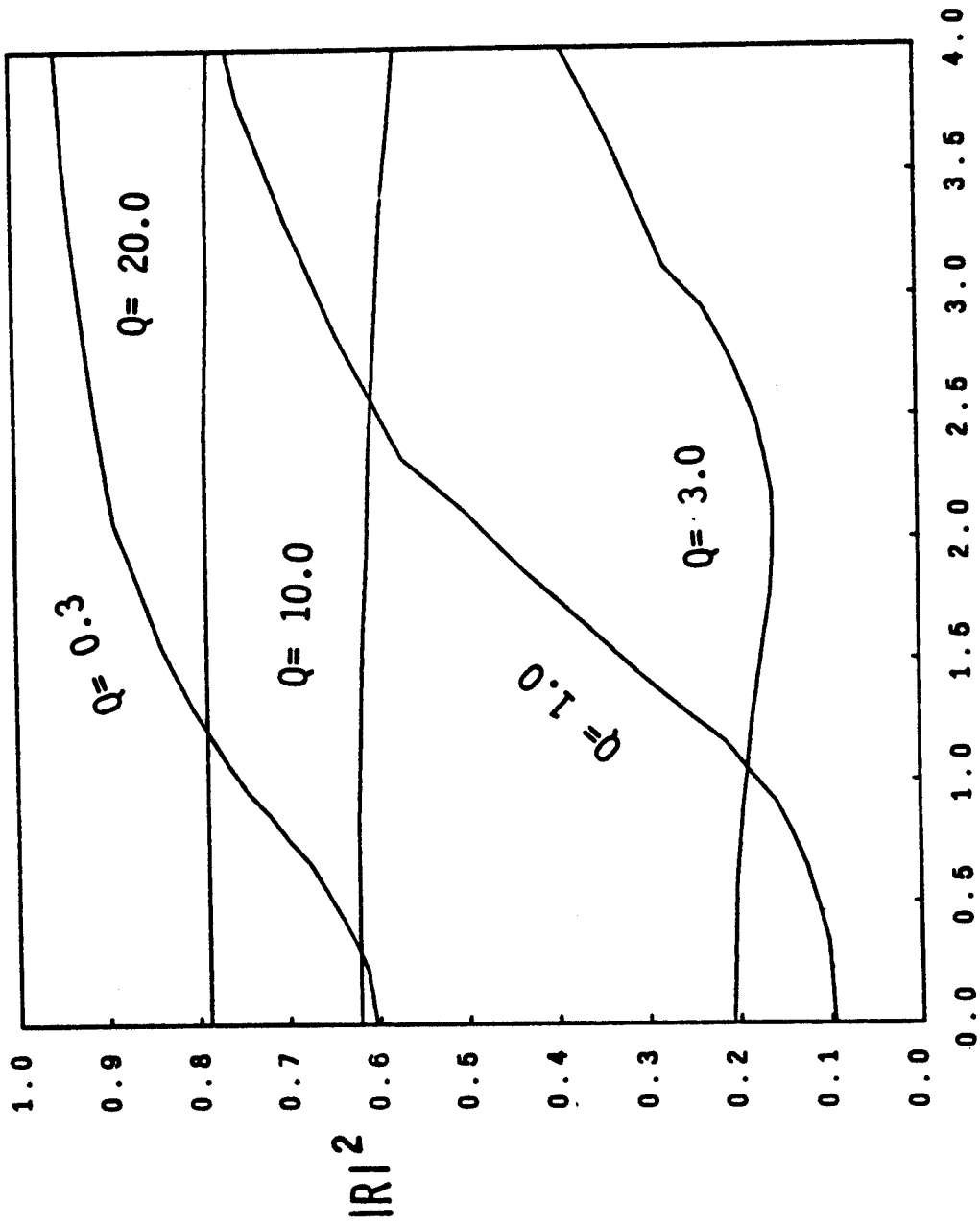
Q= 20.0
Q= 10.0
Q= 3.0
Q= 1.0
Q= 0.3
$|R|^2$
E_1
1.0
0.9
0.8
0.7
0.6
0.5
0.4
0.3
0.2
0.1
0.0
0.0
0.5
1.0
1.5
2.0
2.5
3.0
3.5
4.0

FIG.(6)

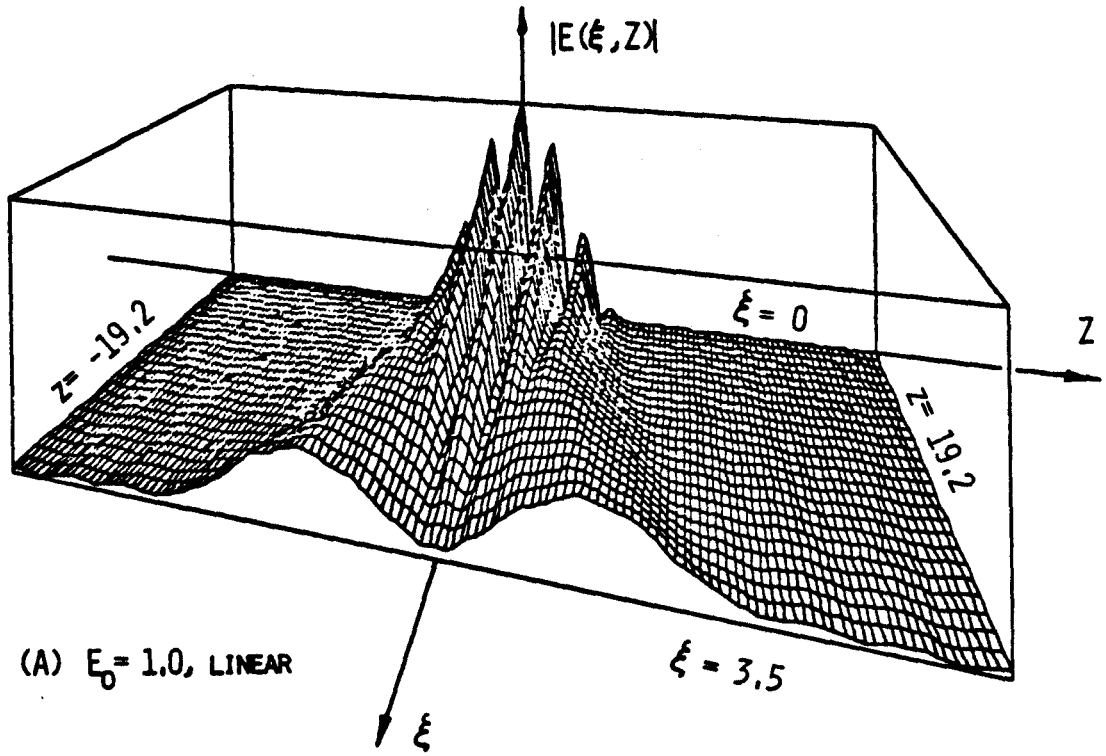

(A) E_0= 1.0, LINEAR

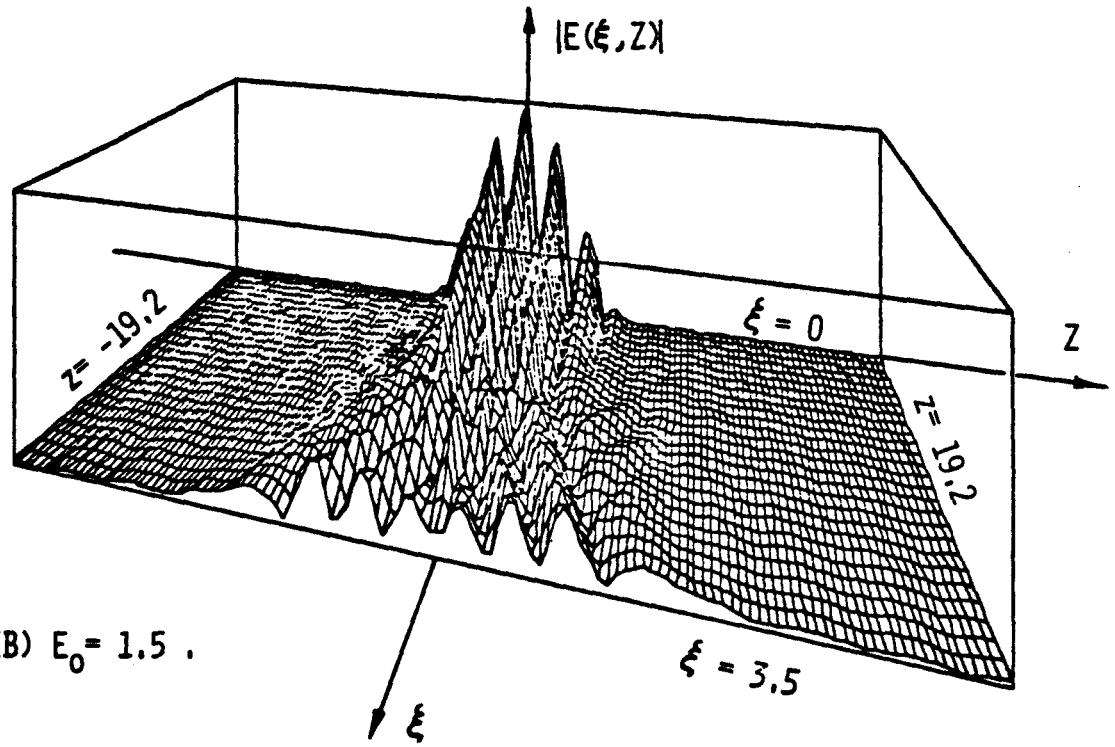

(B) E_0= 1.5 .

FIG.(7)

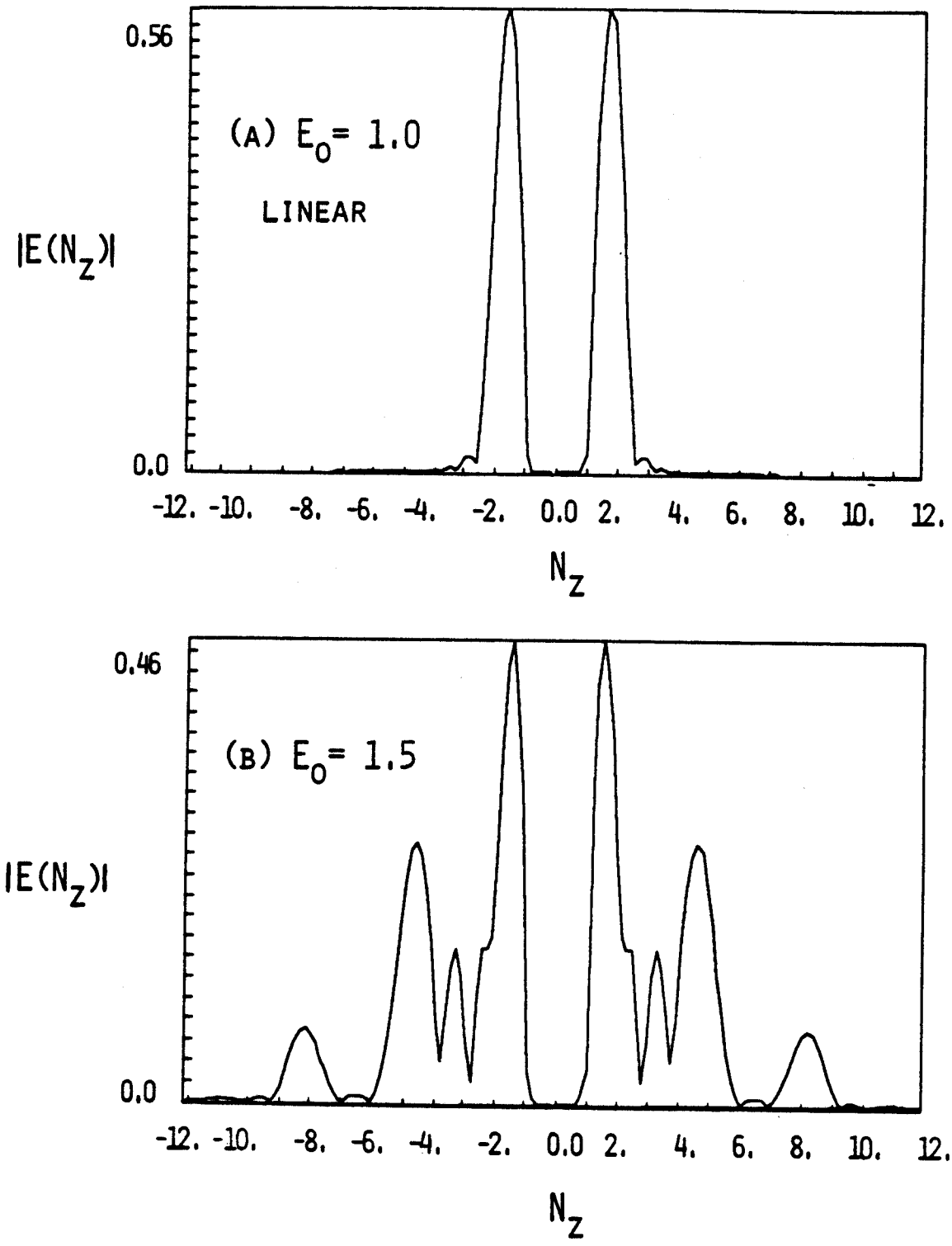
0.56
(A) E_0= 1.0
LINEAR
$|E(N_Z)|$
0.0
-12. -10. -8. -6. -4. -2. 0.0 2. 4. 6. 8. 10. 12.
N_Z
0.46
(B) E_0= 1.5
$|E(N_Z)|$
0.0
-12. -10. -8. -6. -4. -2. 0.0 2. 4. 6. 8. 10. 12.
N_Z

FIG.(8)

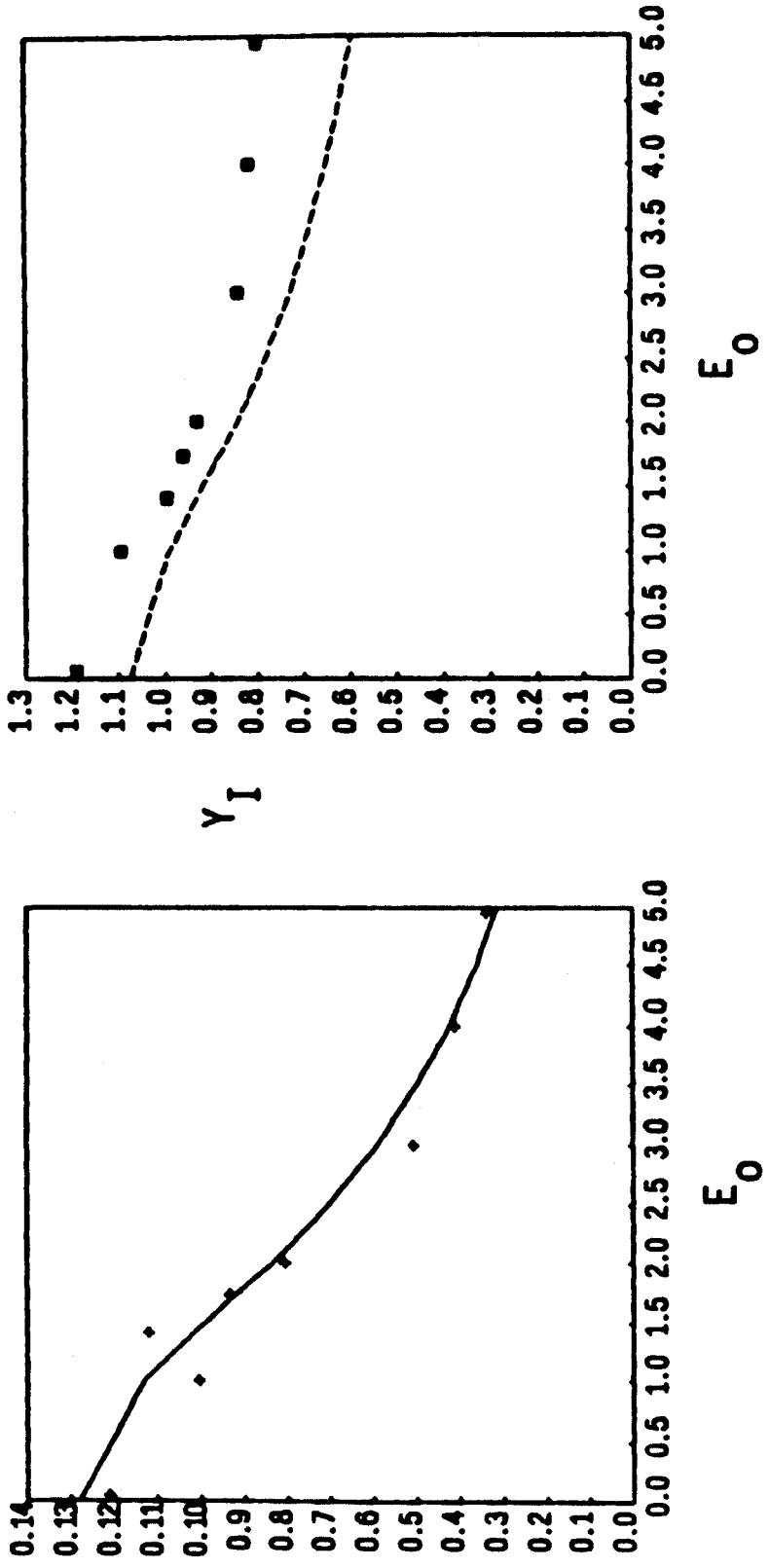
1.3
1.2
1.1
1.0
0.9
0.8
0.7
0.6
0.5
0.4
0.3
0.2
0.1
0.0
Y_I
0.0 0.5 1.0 1.5 2.0 2.5 3.0 3.5 4.0 4.5 5.0
E_o
0.14
0.13
0.12
0.11
0.10
0.9
0.8
0.7
0.6
0.5
0.4
0.3
0.2
0.1
0.0
Y_R
0.0 0.5 1.0 1.5 2.0 2.5 3.0 3.5 4.0 4.5 5.0
E_o

FIG.(9)

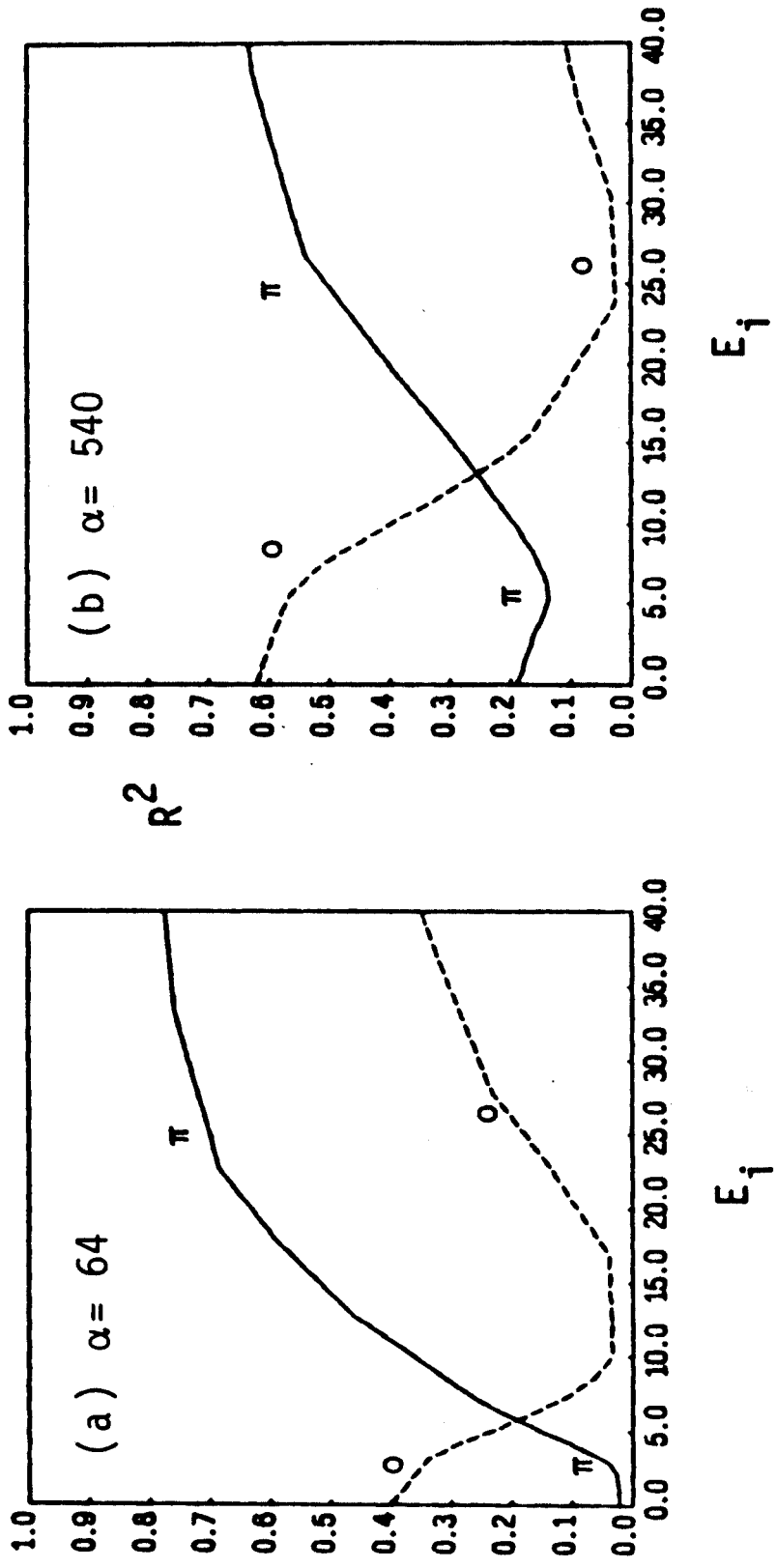
(a) α= 64
(b) α= 540
R2
Ei
π
o
0.0
5.0
10.0
15.0
20.0
25.0
30.0
35.0
40.0
0.1
0.2
0.3
0.4
0.5
0.6
0.7
0.8
0.9
1.0

FIG.(10)

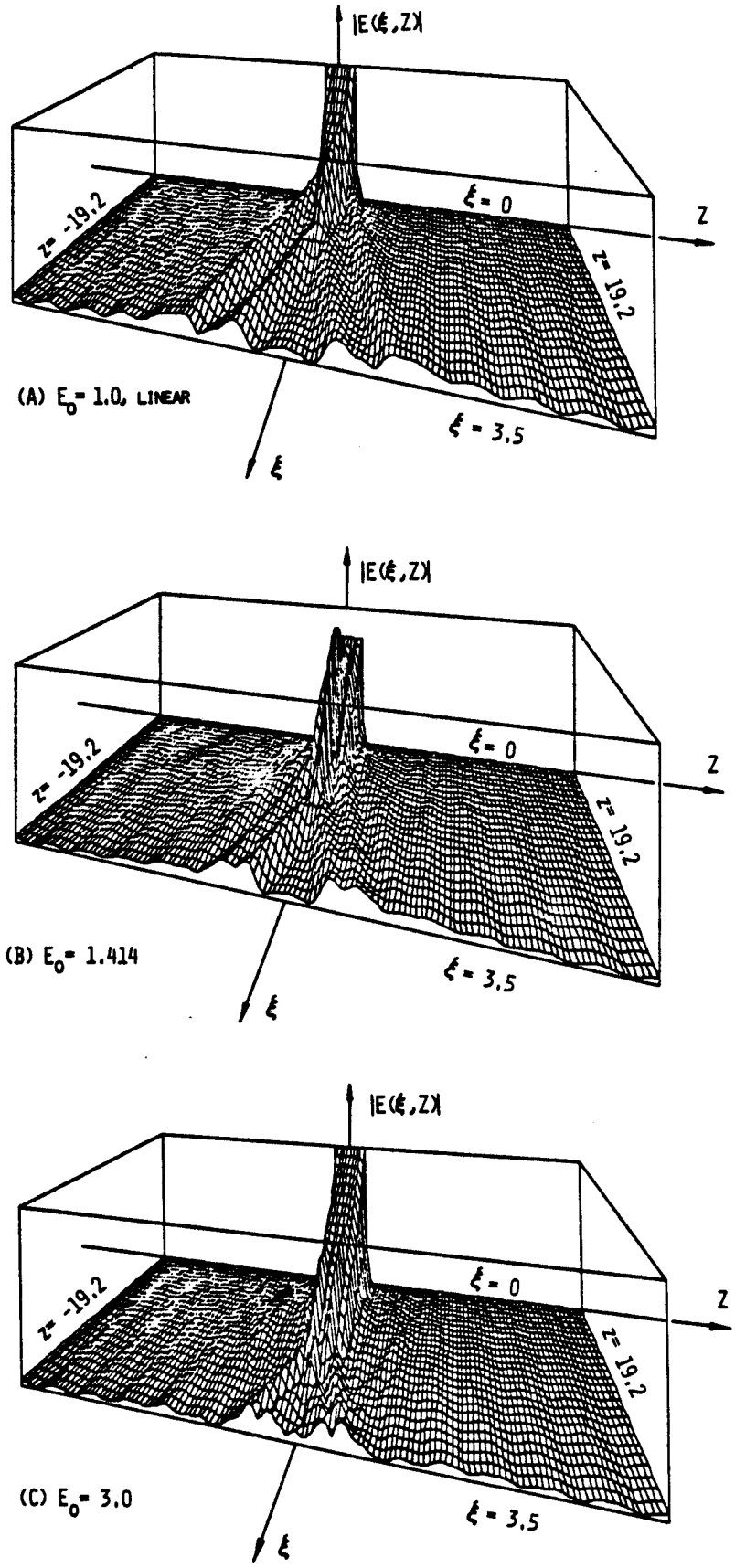
|E(ξ,Z)|
ξ = 0
Z
z= -19.2
z= 19.2
ξ = 3.5
ξ
(A) E_0= 1.0, LINEAR
|E(ξ,Z)|
ξ = 0
Z
z= -19.2
z= 19.2
ξ = 3.5
ξ
(B) E_0= 1.414
|E(ξ,Z)|
ξ = 0
Z
z= -19.2
z= 19.2
ξ = 3.5
ξ
(C) E_0= 3.0

FIG.(11)

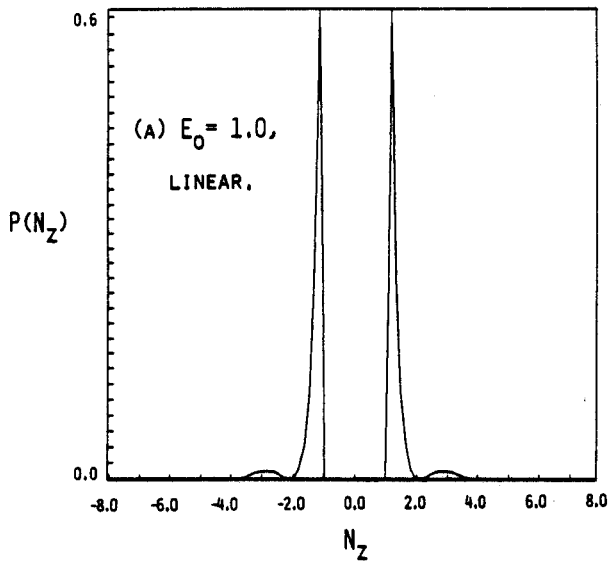
0.6
(A) E_0= 1.0,
LINEAR.
$P(N_Z)$
0.0
-8.0 -6.0 -4.0 -2.0 0.0 2.0 4.0 6.0 8.0
N_Z

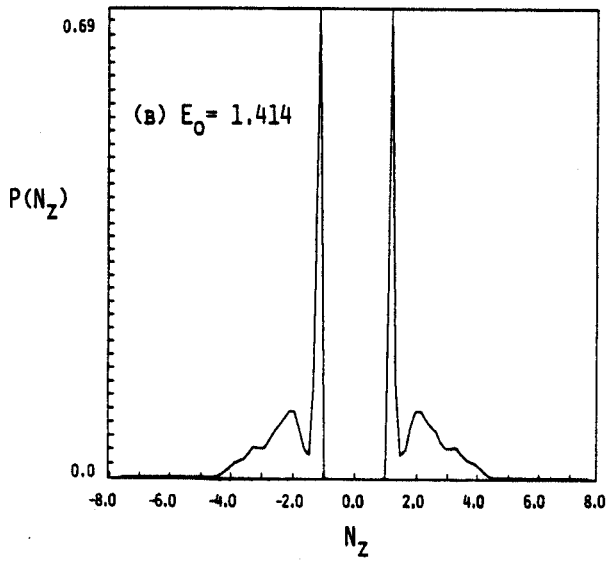
0.69
(B) E_0= 1.414
$P(N_Z)$
0.0
-8.0 -6.0 -4.0 -2.0 0.0 2.0 4.0 6.0 8.0
N_Z

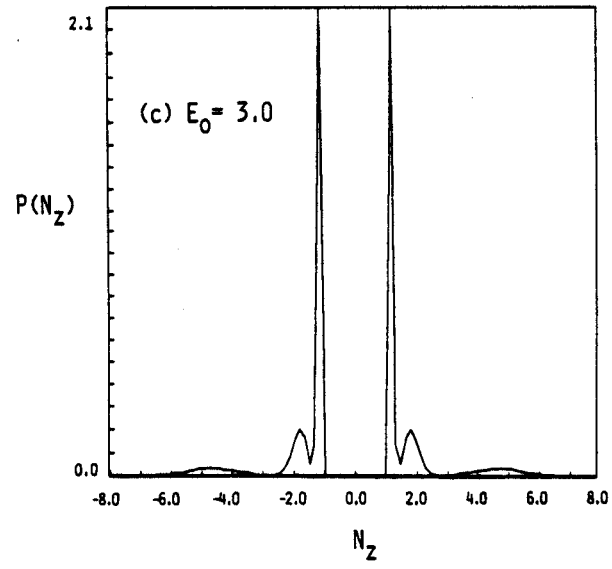
2.1
(c) E_0= 3.0
$P(N_Z)$
0.0
-8.0 -6.0 -4.0 -2.0 0.0 2.0 4.0 6.0 8.0
N_Z

FIG.(12)

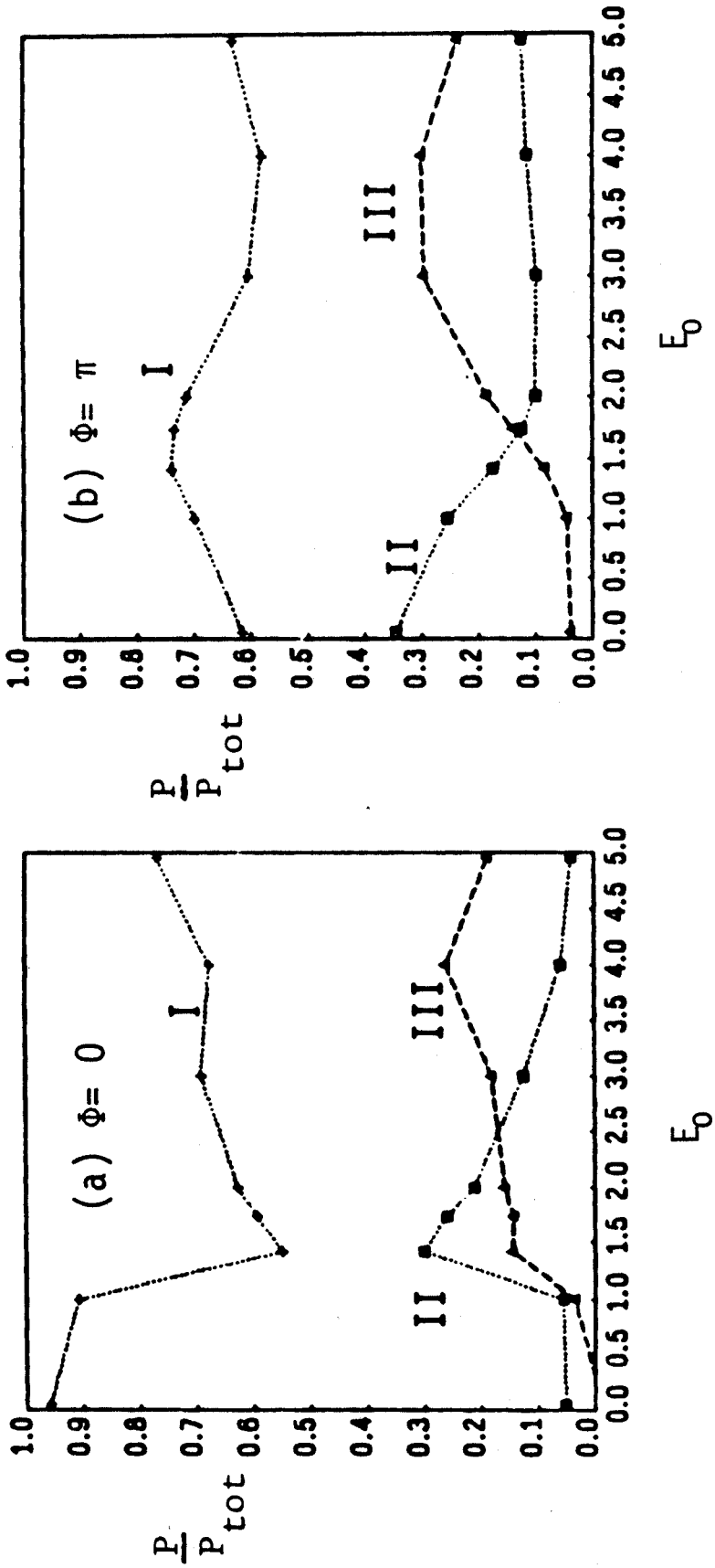
(a) Φ= 0
(b) Φ= π
I
II
III
P/P tot
E0
0.0 0.5 1.0 1.5 2.0 2.5 3.0 3.5 4.0 4.5 5.0
0.0 0.1 0.2 0.3 0.4 0.5 0.6 0.7 0.8 0.9 1.0

FIG.(13)

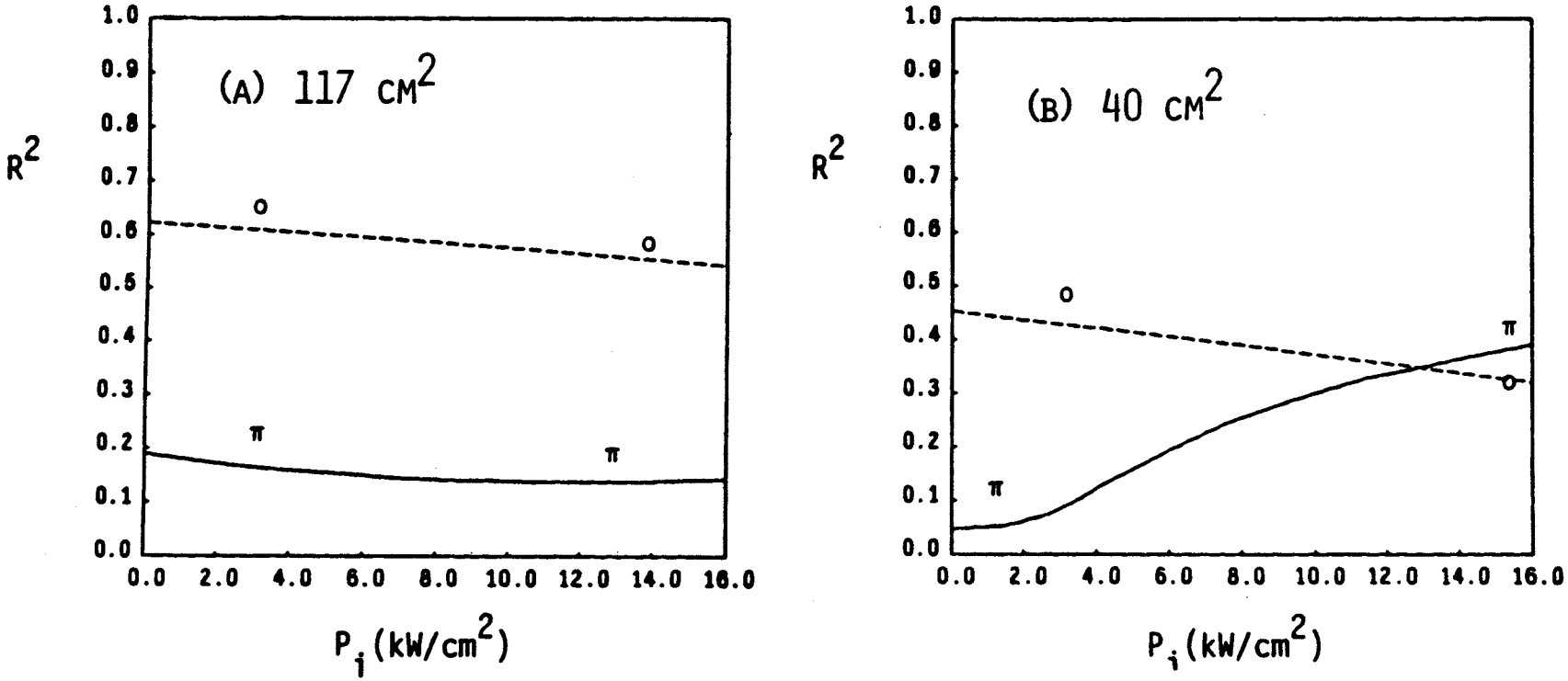
(A) 117 cm^2
(B) 40 cm^2
R^2
P_i (kW/cm^2)
o
π
0.0
0.1
0.2
0.3
0.4
0.5
0.6
0.7
0.8
0.9
1.0
0.0
2.0
4.0
6.0
8.0
10.0
12.0
14.0
16.0

FIG.(14)

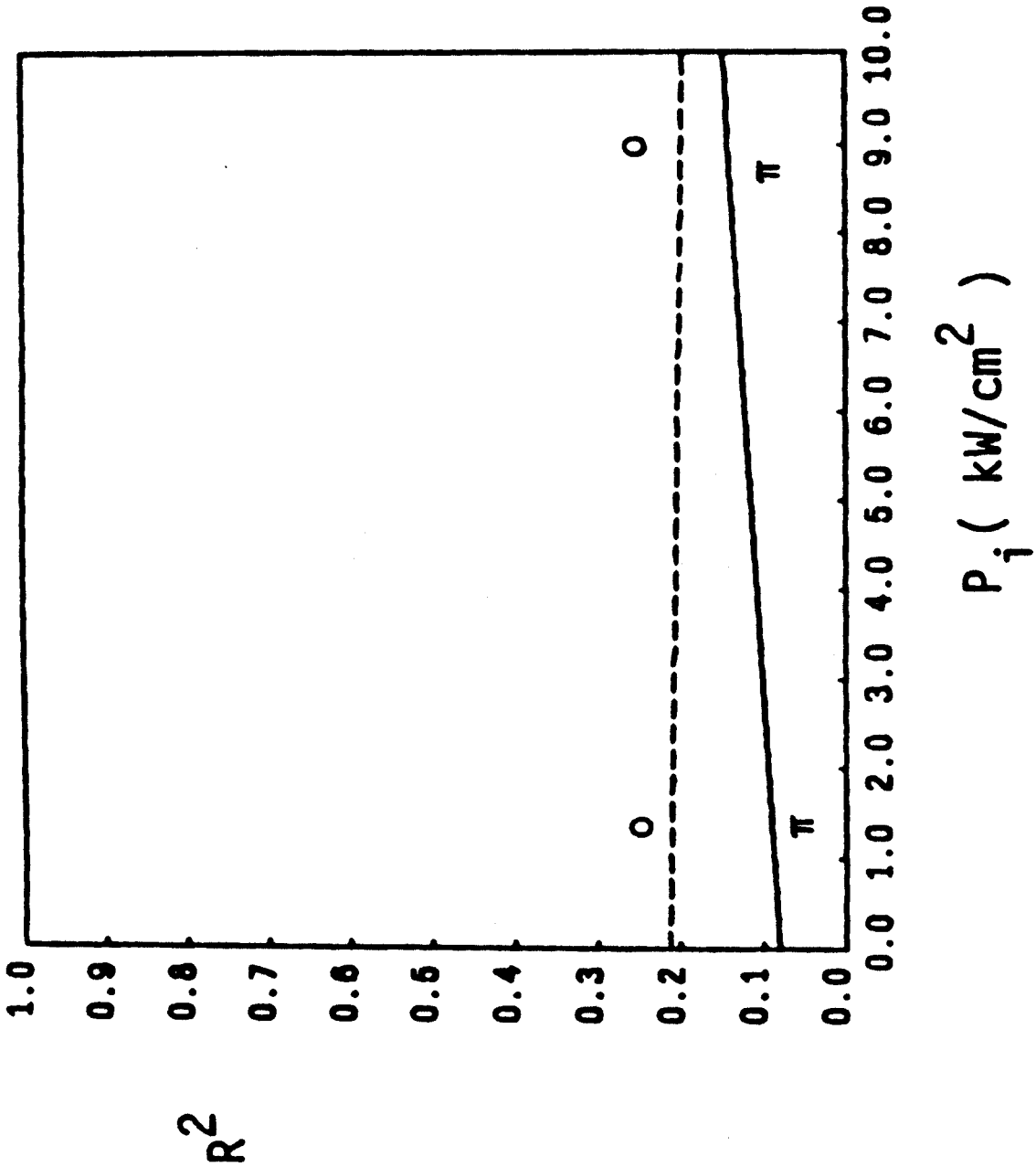
1.0
0.9
0.8
0.7
0.6
0.5
0.4
0.3
0.2
0.1
0.0
R^2
0.0 1.0 2.0 3.0 4.0 5.0 6.0 7.0 8.0 9.0 10.0
P_i (kW/cm^2)
O
O
π
π

FIG.(15)

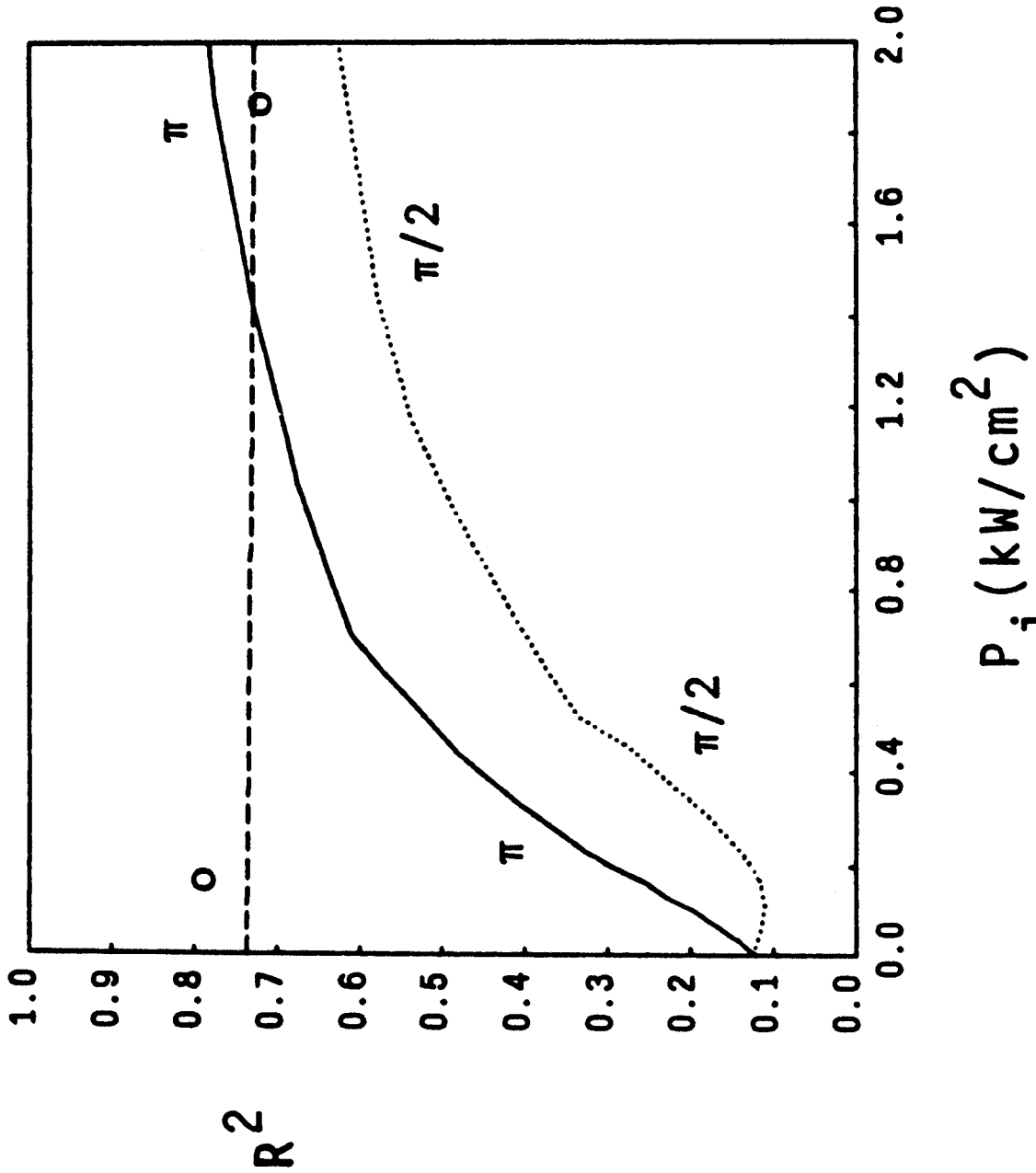
1.0
0.9
0.8
0.7
0.6
0.5
0.4
0.3
0.2
0.1
0.0
R2
0.0
0.4
0.8
1.2
1.6
2.0
Pi (kW/cm2)
π
0
0
π/2
π/2
π

FIG.(16)